

THE INFLUENCE OF SUBSTITUTIONAL ELEMENTS ON THE TRANSFORMABILITY OF 3CR12 STEEL

by

Nils Gene Jungbacke

A thesis submitted to the Faculty of Engineering, University of Cape Town in
partial fulfilment of the degree of Master of Science in Applied Science.

Department of Materials Engineering
University of Cape Town
February 1996

The University of Cape Town has the right to reproduce all or part of this thesis for its own use or in part. Copyright is held by the author.

The copyright of this thesis vests in the author. No quotation from it or information derived from it is to be published without full acknowledgement of the source. The thesis is to be used for private study or non-commercial research purposes only.

Published by the University of Cape Town (UCT) in terms of the non-exclusive license granted to UCT by the author.

ACKNOWLEDGEMENTS

I wish to express my appreciation to all those who assisted me during the course of this project, in particular:

Dr R Knutsen, my supervisor, for his guidance and help throughout my research.

Messrs G Newins, R Hendricks and N Dreze for their help in the workshop, Messrs B Greeves and J Peterson for photographic work, Mr D Dean for assistance with electrical equipment, and Mrs M Topic for laboratory assistance.

Mr D Rickard for assistance with the electron microprobe, Mr M Jaffer for help with the transmission electron microscope, and Mr M Rolfe for computer programming.

Mrs J Sharland, Mrs A Ball and Mrs B Arthur for their administrative support.

The staff and students in the Department of Materials Engineering for their assistance and support.

Columbus Stainless Steel for financial and material support, and the University of Cape Town and the Foundation for Research Development for financial support.

Finally, my family, for their love and support.

SYNOPSIS

An investigation has been carried out on a dual-phase 12 % chromium steel, designated 3CR12, with the aim of developing its composition to improve its properties. By the addition of appropriate alloying elements, it was hoped to produce a fully austenitic structure in the rolling temperature range, and at the same time to enhance the kinetics of the decomposition of austenite so that a fully ferritic structure could be obtained after air cooling. The absence of delta ferrite during hot rolling would eliminate the highly anisotropic structure currently found in 3CR12, whilst accelerating the transformation to alpha ferrite might eliminate the need for an annealing treatment.

Volume fraction analysis (VFA) of specimens quenched from a soaking temperature of 1000°C showed that Co, Ni and Cu stabilise austenite, whilst Si and Al have the opposite effect. These results were confirmed by finding the equilibrium transformation temperatures of the decomposition of austenite to ferrite using dilatometry, and by investigating the partition of alloying elements between delta ferrite and austenite at 1000°C using the electron microprobe.

The effects of the alloying elements on the kinetics of the transformation were investigated by VFA of specimens transformed from 1000°C, and by the use of dilatometry. Dilatometry was used to find the slowest cooling rate at which the alloy was fully untransformed. It was found that Si and Al enhance the kinetics of transformation, whilst Co, Ni and Cu hinder them. The effect of each element is discussed with respect to three factors: the delta ferrite content prior to the transformation, the temperature range of transformation, and the thermodynamic effects of the element.

CONTENTS

	<u>Page</u>
ACKNOWLEDGEMENTS	
SYNOPSIS	
CHAPTER 1 INTRODUCTION	1
1.1 GENERAL INTRODUCTION	1
1.2 ATTAINING THE OBJECTIVES	1
CHAPTER 2 LITERATURE SURVEY	3
2.1 PHYSICAL METALLURGY AND PROPERTIES OF 3CR12	3
2.1.1 Development of 3CR12	3
2.1.2 Microstructure and Properties of 3CR12	5
2.1.3 Impact Toughness and Anisotropy in 3CR12	9
2.1.4 The $\gamma \rightarrow \alpha$ Transformation in 3CR12	13
2.2 EFFECTS OF ALLOYING ELEMENTS ON HIGH TEMPERATURE PHASE STABILITY	17
2.2.1 High Temperature Delta Ferrite Content	19
2.2.2 Effects of the Elements on the A_{c1} Temperature	21
2.3 THE EFFECTS OF ALLOYING ELEMENTS ON THE TRANSFORMATION RATE	22
2.3.1 How Alloying Elements Affect Nucleation and Growth Kinetics	22
2.3.2 The Effect of Specific Alloying Elements on the Transformation Rate	29

CHAPTER 3	EXPERIMENTAL MATERIALS AND METHODS	33
3.1	EXPERIMENTAL MATERIALS	33
3.1.1	Alloy Compositions	33
3.1.2	Production Route	34
3.2	EXPERIMENTAL PROCEDURES	34
3.2.1	Dilatometry	34
3.2.2	Metallography	39
3.2.3	Volume Fraction Analysis	40
3.2.4	Compositional Analysis	41
3.2.5	Laboratory Hot Rolling	42
3.2.6	Mechanical Properties	42
CHAPTER 4	EXPERIMENTAL RESULTS	43
4.1	ASPECTS OF THE $\gamma \rightarrow \alpha$ TRANSFORMATION	43
4.1.1	Epitaxial Growth	43
4.1.2	Delta Ferrite Content and the Resulting Microstructural Anisotropy	45
4.1.3	Precipitation During Cooling from 1000°C	47
4.1.4	Element Partition During Transformation	49
4.2	ALLOYING ELEMENTS AND HIGH TEMPERATURE PHASE STABILITY	50
4.2.1	Delta Ferrite / Austenite Content at 1000°C	50
4.2.2	The Ae_1 and Ae_3 Temperatures of the Alloys	53
4.2.3	Partition of Alloying Elements at 1000°C	54
4.3	ALLOYING ELEMENTS AND THE RATE OF TRANSFORMATION	56
4.3.1	Extent of Austenite Decomposition After Cooling at 1°C/min	56

4.3.2	Critical Cooling Rates for the Initiation of Transformation	61
4.3.3	The Effect of Delta Ferrite Content on the Transformation Rate	62
4.4	MECHANICAL PROPERTIES OF 3CR12	66
4.4.1	Impact Testing Results	66
4.4.2	Tensile Properties	68
CHAPTER 5	ANALYSIS	69
5.1	AUSTENITE / FERRITE FORMING ABILITIES OF THE ELEMENTS	69
5.1.1	Multiple Regression Analysis	69
5.1.2	Free Energy and Crystal Structure	71
5.2	KINETICS OF THE $\gamma \rightarrow \alpha$ TRANSFORMATION IN 3CR12	72
5.2.1	Regression Analysis of Transformation Rate Results	72
5.2.2	Comparison of the Methods Used to Measure Transformation Kinetics of the Alloys	74
5.2.3	Initial Ferrite Content and the Transformation Rate	77
5.2.4	Transformation Temperature and Kinetics	84
5.2.5	Summary	87
5.3	DISCUSSION OF MECHANICAL PROPERTY RESULTS	88
5.3.1	Toughness and Specimen Orientation	88
5.3.2	Regression Analysis of Tensile Results	89
CHAPTER 6	CONCLUSIONS	90
6.1	EFFECTS OF THE ELEMENTS	90
6.2	GENERAL CONCLUSIONS	91
REFERENCES		92

1. INTRODUCTION

1.1 GENERAL INTRODUCTION

3CR12 is an acronym for chromium containing corrosion resistant 12-chromium steel. The alloy is produced by Columbus Stainless at their plant in Middelburg. This thesis forms part of the investigation into the development of a new version of 3CR12.

The primary objective of this research is to develop the composition of 3CR12 to obtain a unique combination of properties. A fully ferritic equiaxed microstructure is required directly after hot rolling and air cooling, with no annealing treatment. The alloy will have to transform fully at cooling rates of up to $15^{\circ}\text{C} / \text{min}$, the speed at which the outside of a rolled coil has been measured to cool at the Columbus Mill. Good weldability, and mechanical properties equal to or better than those of conventional 3CR12, must also be obtained.

1.2 ATTAINING THE OBJECTIVES

In the past, the microstructure of hot rolled and air cooled plates of 3CR12 consisted of elongated ferrite and martensite colonies. The mechanical properties were thus anisotropic, and an expensive and time consuming anneal was necessary to provide adequate ductility. This treatment had little effect on the anisotropy.

The hot rolled, air cooled structure of 3CR12 arises as follows. The hot working takes place over the temperature range $1200 - 800^{\circ}\text{C}$. Over a significant portion of this range, 3CR12 has a two phase microstructure of austenite and delta ferrite. During the deformation, the grains of both phases become extended in the rolling direction. At around 800°C , the decomposition of austenite to ferrite begins. The alpha ferrite grows simply by migration of the original delta ferrite / austenite interphase boundaries. As a result, the highly elongated delta ferrite morphology is retained.

As previously mentioned, the outside of a rolled coil cools at up to $15^{\circ}\text{C} / \text{min}$. However, 3CR12 requires cooling rates of less than $5^{\circ}\text{C} / \text{min}$ to transform fully. Consequently, significant amounts of martensite are present after air cooling.

Thus, in order to fulfill the aims of this thesis, two clear objectives are defined. The first objective is to minimise the amount of delta ferrite present in the alloy during rolling. If a fully austenitic structure could be obtained, alpha ferrite would have to nucleate and grow from austenite grain boundaries. This would eliminate the problem of the retention of the elongated delta ferrite structure arising from boundary migration. Decreasing the delta ferrite content below a certain level would probably also have the desired effect. Smaller delta ferrite grains would have a shorter length after deformation than larger ones. As a result, the extent of the elongation, and the resulting anisotropy, would be less. Also, some nucleation at austenite grain boundaries might occur in the regions between the delta ferrite grains. The first objective could be achieved by the addition of elements which stabilise the austenite phase.

The second objective is to increase the cooling rate at which 3CR12 is able to transform to a fully ferritic structure after hot rolling to as close to $15^{\circ}\text{C} / \text{min}$ as possible. The need for an annealing treatment would then be eliminated. This objective could be achieved by the addition of elements which accelerate the transformation to ferrite.

2. LITERATURE SURVEY

This chapter is a review of the literature relevant to the objectives, results and analysis of this thesis. The first section of this survey discusses the development, microstructure and properties of 3CR12. The second part looks at the austenite / ferrite phase balance in stainless steels and how it is affected by alloying elements. Finally, section three discusses the consequences of the addition of alloying elements on the kinetics of the decomposition of austenite in ferrous alloys.

2.1 PHYSICAL METALLURGY AND PROPERTIES OF 3CR12

2.1.1 Development of 3CR12

3CR12 was developed in the late 1970's from AISI 409 ferritic stainless steel. The work was performed by Middelburg Steel & Alloys (MS&A), the forerunner of Columbus Stainless. Prior to the introduction of 3CR12, ferritic stainless steels were considered by many developmental organisations to be a promising replacement for mild steel in corrosive environments. However, many of these alloys had serious deficiencies in ductility, toughness, formability and weldability [1]. MS&A began the development of a tough, weldable version of type 409. The results of several major studies [2, 3] led to the conclusion that excessive grain growth and the interstitial elements, carbon and nitrogen, were the most significant causes behind the inferior properties of the ferritic stainless steels. The focus of research turned to the reduction in the amount of interstitial elements and the development of a stable, fine-grained microstructure.

The interstitial levels for 3CR12 were set at 0,025 % for carbon and 0,02 % for nitrogen (unless otherwise stated, all compositions in this thesis are given in weight percent), the minimum which can be economically achieved by conventional metallurgical processes. The most important compositional deviations from type 409 (see table 2.1 on page 5) are a reduction in the amounts of the ferrite forming

elements, silicon and titanium. The duplex ferrite / austenite structure thus found during rolling is responsible for the fine, stable microstructure of 3CR12 [1].

In the mid-1980's, the development of 3CR12 was taken a step further [4]. At the time, 10 to 15% of production heats were found to be difficult to soften or to have variable properties after annealing. These heats had to be re-annealed, which slowed down production and increased costs. Samples taken from production heats *before annealing* were studied in an effort to solve the problem. Results showed that small coils were hard along their full length, whilst large coils were soft for most of their length, with one or two hard laps on the inside and outside. These findings could easily be explained by the geometry of the coils and heat conduction. Heat is conducted more slowly from the middle of a coil, which results in "self-annealing". Self-annealed coils were tested briefly in the marketplace, and no problems were reported. In 1987, excess demand led to further investigation into the self-annealing process. An insulating blanket was placed over the coil as it came off the downcoiler. This resulted in uniform properties throughout the coil, which were within specifications. The blankets were soon replaced by specially designed insulating hoods.

Work performed at the University of Pretoria [5, 6] showed that the term self-annealed was a misnomer. Van Rooyen used continuous cooling transformation diagrams to show that the slower cooling rate simply allows a greater proportion of ferrite to form, resulting in a fully soft coil. Further work at the University of Pretoria showed that titanium and nickel additions were not necessary to obtain typical 3CR12 properties. Alternative suitably balanced compositions could be used to obtain equally good results. The elimination of titanium would also lead to a reduction in the level of surface defects. It was calculated that lower alloy costs, yield gains, and elimination of the annealing process would lead to savings of more than twenty percent. In February 1989, the decision was taken to switch to production of 3CR12L (see table 2.1), and in 1991, production tonnages passed the 60 kt level.

As discussed in the introduction, 3CR12 has entered a new phase in its development. The composition is being altered to increase the cooling rate at which the alloy can

transform fully to ferrite. The aim is to eliminate the need for annealing or for insulating hoods. In addition, the composition is being designed to produce a fully, or nearly fully, austenitic structure during rolling, to try and eliminate the anisotropic properties currently found in 3CR12.

Table 2.1 The compositional development of 3CR12.

ALLOY	C	Cr	Mn	Ni	Si	Ti	N
AISI 409	0,025	11,0	1,0	0,5	1,0	0,75	-
3CR12	0,025	11,5	1,2	0,6	0,5	0,3	0,02
3CR12L	0,025	11,5	1,0	0,1	0,5	0	0,02

2.1.2 Microstructure and Properties of 3CR12

2.1.2.1 Microstructural Studies

Soon after the development of 3CR12, Ball and Hoffman [1] studied the microstructure and annealing response of several 3CR12-type alloys. The as-rolled microstructure was reported to consist of a banded two phase structure of martensite and ferrite with numerous precipitates of titanium carbides and nitrides. A series of subcritical annealing treatments was carried out at 725°C, and the extent of recrystallisation monitored by hardness measurements. These tests showed that the alloy had completely recrystallised in 60 seconds. Continued annealing caused little or no further grain growth and a fine, equiaxed ferrite structure remained stable. Transmission electron microscope (TEM) studies showed the presence of numerous impurity particles both at the grain boundaries, which were frequently puckered or pinned by precipitates, and within grains. Energy dispersive spectroscopy (EDS) showed that all the precipitates contained titanium and phosphorous, whilst some contained nickel.

The stability of the fine grained ferrite structure formed by subcritical annealing was ascribed largely to the duplex ferrite / austenite structure present during rolling, which would result in a very uniform state of plastic deformation. On cooling, a fine ferrite grain size would result. Following annealing, a fine recrystallised structure is

produced, and the pinning of grain boundaries by precipitates prevents deleterious grain growth. If annealing is carried out in the duplex region (above 800°C), the growth of austenite grains at the boundaries also inhibits ferrite grain growth.

The austenitisation reaction in 3CR12 was studied further by Ball et al [7]. Dilatometry showed that austenite is stable in 3CR12 from 800°C to 1350°C. As the holding temperature was raised from 800°C, the volume fraction of austenite increased to a maximum of 0,92 at 1050°C, before decreasing continuously to zero at 1350°C. The transformation to austenite was found to be controlled by diffusional growth, as distinguished from the nucleation event, and to be independent of the dissolution of carbides.

2.1.2.2 Tensile Properties

Brink [8] studied the tensile properties of 3CR12 as a function of annealing temperature. After a prior anneal at 1000°C, specimens were soaked for an hour at various temperatures over the range 25 - 1050°C, and then furnace cooled (see figure 2.1). Ductility reaches a maximum, and tensile strength and proof stress a minimum, at an annealing temperature of around 800°C.

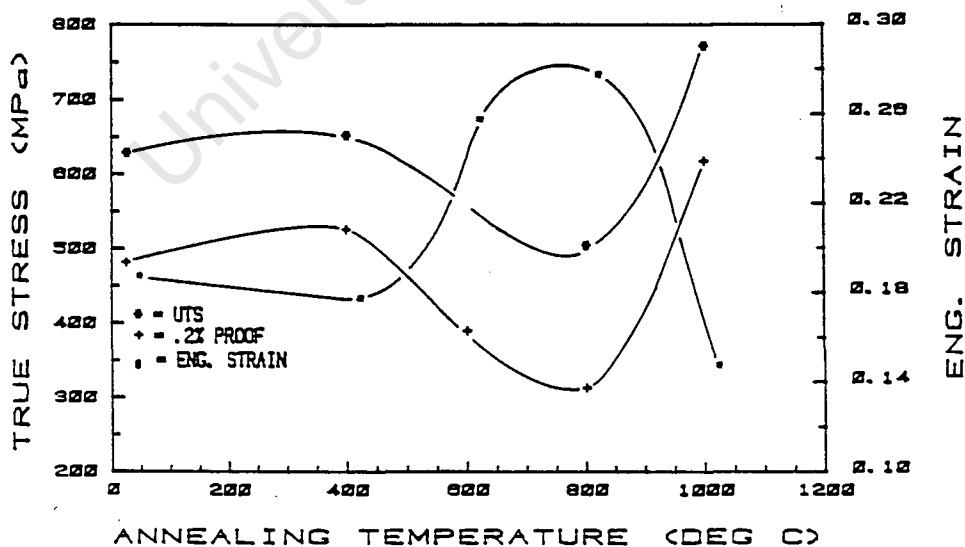


Figure 2.1 Tensile properties of 3CR12 as a function of annealing temperature (after reference 8).

2.1.2.3 Welding Metallurgy

The weldability of 3CR12, and of a nickel rich version 3CR12Ni (1,2 % Ni), was investigated by Hoffman [9]. It was found that 3CR12Ni had superior welding properties to conventional 3CR12. This was ascribed to the presence of large amounts of martensite (austenite during welding) in the heat affected zone (HAZ). Up to 90 % volume fraction martensite was found in 3CR12Ni, whilst a maximum of 40 % was found in 3CR12, mainly at ferrite grain boundaries. The martensite is of the low carbon lath type and is inherently tough. It was also found that the presence of the austenite at elevated temperatures restricted ferrite grain growth in the HAZ.

After a specific welding treatment, it was found that the presence of only 15 % martensite in the HAZ of a 3CR12 weld lead to considerable grain growth and inadequate impact energies (20 J). The 3CR12Ni alloy, after undergoing the same treatment, had approximately 80 % martensite in the HAZ, no visible grain growth, and excellent toughness. It was concluded that 3CR12-type alloys can be welded in sections up to and including 32 mm provided the steel has a minimum of 40 % martensite in the HAZ.

The toughness of the HAZ in 3CR12 weldments was also investigated by Zaayman and Van Rooyen [10]. They found that the presence of even small amounts of delta ferrite in the HAZ was detrimental and acceptable ductile brittle transition temperatures (DBTT) were obtained only when the HAZ had a fully martensitic structure.

2.1.2.4 Deformation and Recrystallisation

Prozzi and Van Rooyen [11] investigated the recrystallisation behaviour of 3CR12 after plane strain compression. Prior to deformation, the specimens were heat treated at 1200°C for 30 minutes and furnace cooled, thus producing an equiaxed ferritic starting microstructure. Following this, specimens were heated to 1000°C and held at this temperature for 10 minutes to produce a stable phase balance of 15 % ferrite and 85 % austenite. A sample was then subjected to a compressive true strain of 50 %, followed by rapid cooling. The delta ferrite grains were found to be highly deformed

perpendicular to the main direction of stress, and a distinctive network of subgrains indicated that recovery and recrystallisation had taken place (see figure 2.2a). Dynamic recrystallisation has previously been shown to occur in ferritic [12] and dual phase [13] stainless steels. When the temperature of the specimen was maintained at 1000°C for one minute after deformation, followed by rapid cooling, subgrain growth occurred within the delta ferrite, and resulted in the partitioning of the ferrite bands by transverse grain boundaries (see figure 2.2b). The interphase boundaries, however, remain elongated.

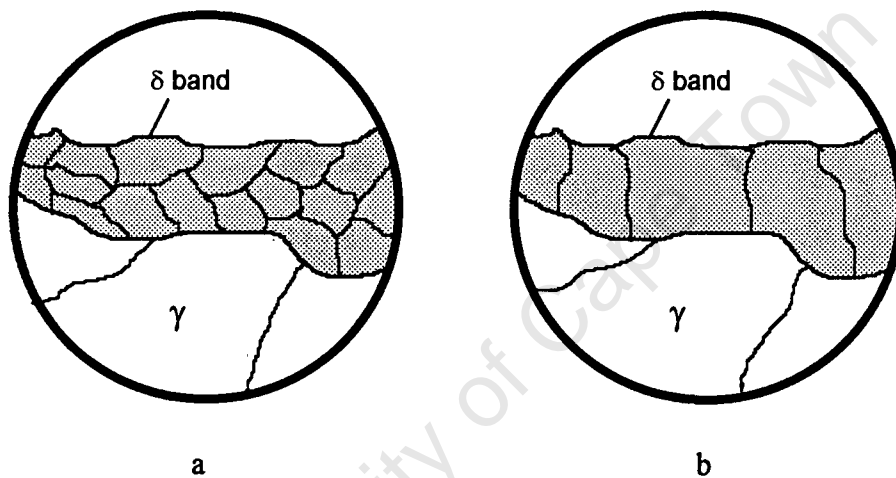


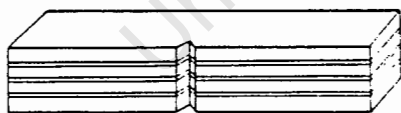
Figure 2.2 a) Recrystallised δ -ferrite grain after 0,5 compressive true strain at 1000°C.
b) Grain growth has occurred after the specimen was held at 1000°C for one minute after compression.

After deformation at 1000°C, specimens were also slowly cooled in order to allow the decomposition of austenite to take place. Epitaxial growth of the existing recrystallised delta ferrite grains into the austenite produced what Prozzi described as an equiaxed ferrite microstructure. The ferrite grain size was found to have decreased relative to the undeformed material. An increase in the amount of deformation led to a slightly finer structure.

2.1.3 Impact Toughness and Anisotropy in 3CR12

The effect of specimen orientation on the impact toughness of 3CR12 has been quite extensively investigated. Studies have been performed on all four of the orientations shown overleaf in figure 2.3. Grobler and Van Rooyen [14] investigated the toughness of specimens tested in the L-T and S-L orientations. The ductile-to-brittle transition temperatures were found to be 112°C for the S-L orientation, and -64°C for the L-T orientation. A ductile fibrous (observed at 10X magnification) fracture surface was observed for the S-L specimens, whilst the L-T surfaces were characterised by a number of small splits parallel to the rolling plane, perpendicular to the direction of propagation of the main crack. As the testing temperature was decreased, the number of splits increased. Metallography showed that the splits propagated by decohesion of elongated ferrite / ferrite and ferrite / martensite boundaries, as well as by transgranular cleavage. By limiting the applied impact energy to 30J, Grobler and Van Rooyen showed that delamination perpendicular to the direction of the main fracture occurs prior to the initiation of the principal crack. Thus splitting occurs ahead of the propagation of the main crack, and the principal fracture was found to occur by ductile fracture of the thinner specimens created by splitting.

The splitting phenomenon can be compared to the fracture of “crack-divider” laminated Charpy specimens. Embury et al [15] prepared standard sized Charpy specimens containing up to six layers of mild steel. The DBTT's and shelf energies



*“Crack-divider” Charpy specimen
(after reference 15)*

were found to decrease as the number of “crack-dividing” layers increased, and examination of the fracture surfaces showed that a pair of shear lips formed on each subunit. Because of the pancake shaped grain morphology of rolled 3CR12, a L-T (or a T-L) Charpy specimen can be considered as a crack-divider specimen. During Charpy impact testing, plastic deformation at the root of the notch is highly constrained, and a triaxial stress state develops. If the principal tensile stress is below

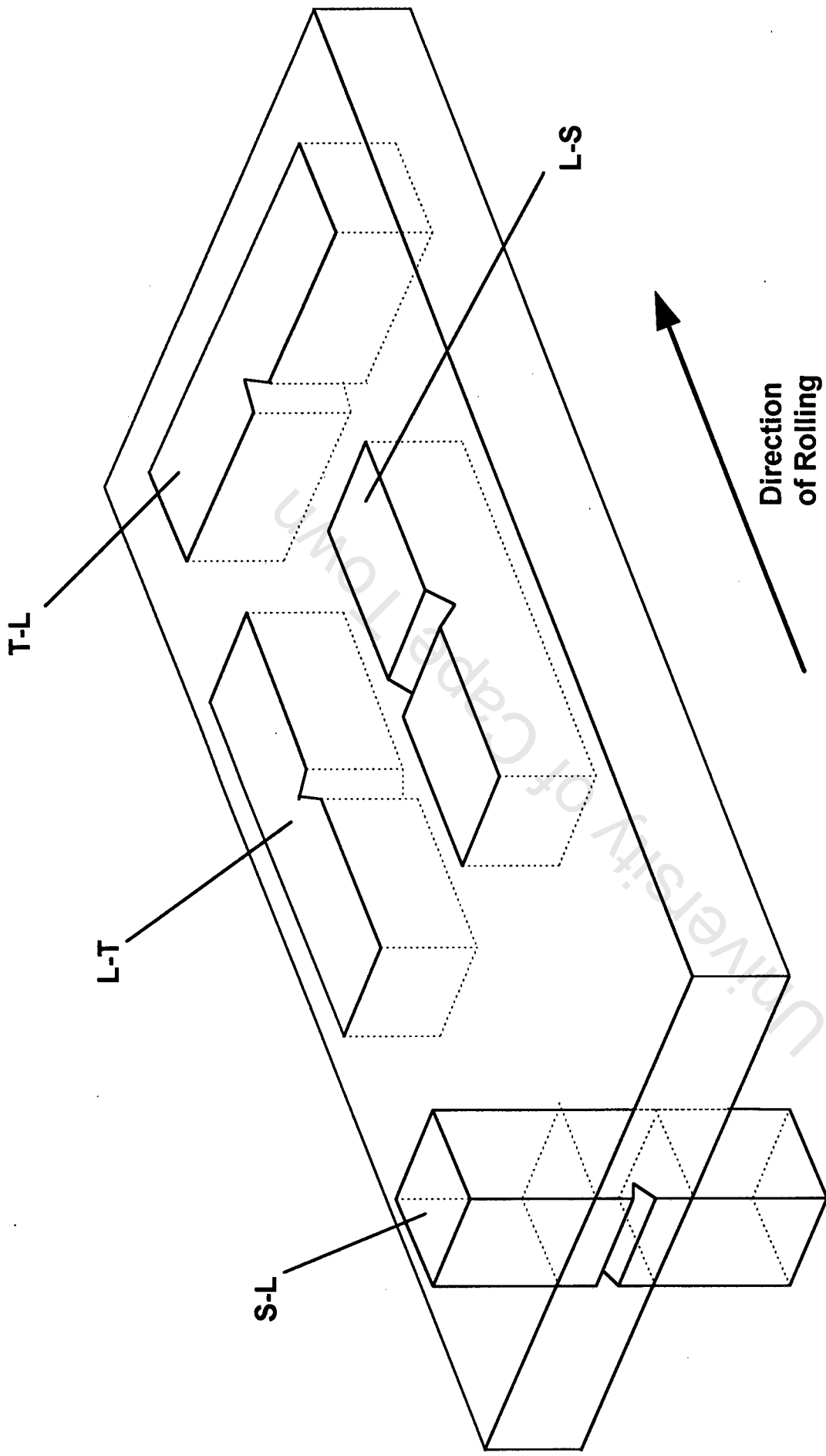


Figure 2.3: Orientation of Charpy specimens with respect to the direction of rolling. The notation used is as follows:

First letter: axis of specimen

Second letter: direction of propagation of fracture

the stress required to cause transverse fracture, and the tensile stress perpendicular to the direction of splitting exceeds the fracture strength required for splitting, splitting will precede transverse fracture.

Any local split will cause a relaxation of the local triaxial stress condition in the vicinity of the split. This reduction of the maximum stress at the notch will reduce the temperature at which cleavage fracture can be expected, and therefore also the DBTT. However, the reduction in the stress will also reduce the upper shelf impact energy.

Cortie et al [16] investigated the impact toughness of L-T and L-S ("crack-arrestor") 3CR12 specimens, and observed different fracture modes for the two orientations. The L-T specimens exhibited delamination, as found by Grobler and Van Rooyen. The failure of the L-S specimens was described as follows. The state of triaxial stress formed at the tip of the advancing crack pulls apart the banded microstructure of the material. This decohesion perpendicular to the direction of failure results in the blunting of the crack and a reduction in the triaxiality of stresses at the crack tip. As a result, the L-S orientation was found to have a lower DBTT and higher shelf energies than the L-T orientation.

Matthews et al [17] obtained values for the impact toughness of 3CR12 in the T-L and L-T orientations, as well as for specimens at an intermediate orientation of 45 degrees to the rolling direction. At all three testing temperatures (-22, 0, and 22°C), the ascending order of toughness was found to be T-L, intermediate, L-T. The authors attempted to explain the results using bulk texture analysis.

Bramfitt and Marder [18] investigated delamination in Charpy specimens of low-carbon steel in the T-L and L-T orientations. They found that an increase in the number of laminations (N) led to a decrease in absorbed energy, E, given by the following relationship:

$$E = E_0 / (N + 1),$$

where E_0 is the absorbed energy for an unsplit Charpy specimen, and $(N + 1)$ is the effective number of smaller Charpy specimens created by splitting. They also found

that the higher the aspect ratio of the grains (length to thickness), the lower the shelf energy. The transverse specimens were found to exhibit more laminations for an equivalent test temperature.

University of Cape Town

2.1.4 The $\gamma \rightarrow \alpha$ Transformation in 3CR12

2.1.4.1 Initiation

The initiation of alpha ferrite growth in 3CR12 has been reported by several authors to occur by migration of existing delta ferrite / austenite interphase boundaries [19, 20]. This process, where the alpha ferrite has the same crystal orientation as the existing ferrite and no interface is formed, is also known as epitaxial growth. It must be distinguished from sympathetic nucleation, which has been reported to occur in several steels [21]. This mode of nucleation also involves the growth of alpha ferrite from a delta ferrite / austenite interface, but the orientations of the two crystals would differ, and a boundary would be observed.

The successful nucleation of a new phase at a grain boundary (or otherwise) is largely governed by the decrease in the Gibbs free energy which its formation will cause [22]. A key consideration in the free energy balance is the change in interfacial energy engendered by the new phase. The surface energy of the original boundary is eliminated, but is replaced by the interfacial energy between the new phase and both the grains with which it is in contact. Sympathetic nucleation of alpha ferrite will often be favoured over nucleation at γ / γ boundaries because of the low energy of the δ / α -ferrite interface (see figure 2.4). The two phases have the same crystal structure, and since their compositions will be very similar,

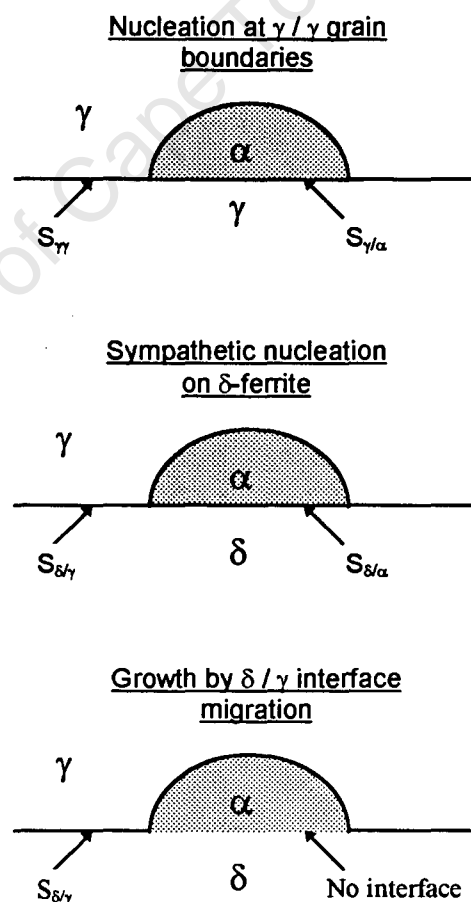


Figure 2.4 The three modes of nucleation of alpha ferrite.

they will have nearly identical lattice parameters. Epitaxial growth, however, should be favoured over sympathetic nucleation. Since there is no boundary between the two ferrite phases, the increase in interfacial energy due to the new phase will be minimised.

2.1.4.2 Growth

The isothermal decomposition of austenite to ferrite was investigated by Ball et al [7], and the TTT diagram determined (see figure 2.5). At 650 and 700°C, new ferrite was seen to grow preferentially from existing delta ferrite grains, with the same crystal orientation. Interphase boundary precipitation of chromium carbides and nitrides was also observed. The growth of ferrite was said to be controlled by the rejection of carbon due to the large difference in the solubility of the element in the two phases. At 750°C, irregular or convoluted ferrite grains were seen to be growing into the austenite, and interphase boundary precipitation was not observed. At this temperature, the solubility and diffusivity of carbon does not require carbides to be precipitated at the interface, and the growth of ferrite proceeds more quickly. At 800°C, no significant growth of ferrite was observed.

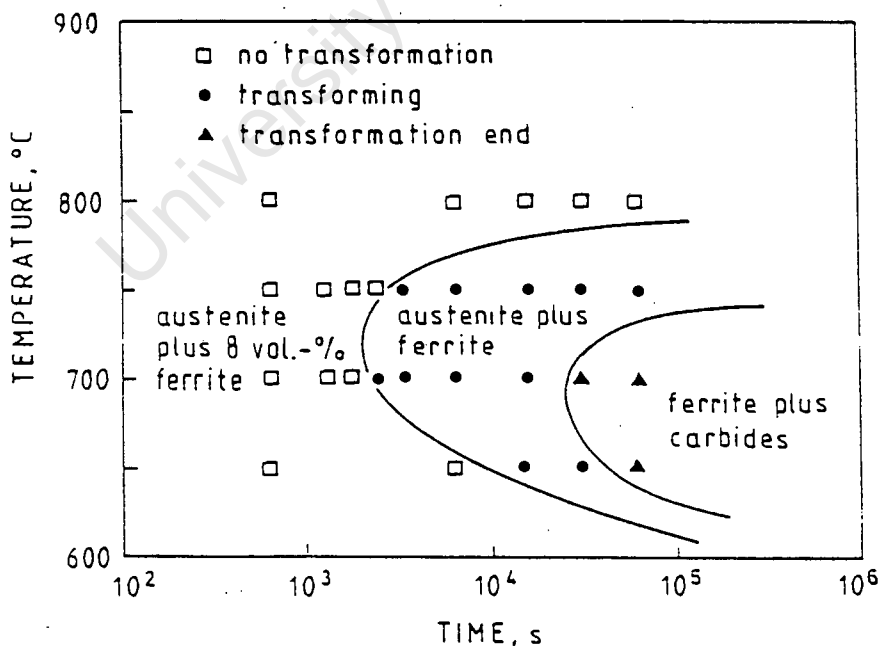


Figure 2.5 The TTT diagram for the decomposition of austenite to ferrite plus carbides in 3CR12 (after reference 7).

Knutsen [20] studied the evolution of the microstructure of 3CR12 from the single phase delta ferrite region at 1380°C, through the dual-phase δ / γ region, to the room temperature microstructure of alpha ferrite and martensite (see figure 2.6). The microstructure at 950°C, found by quenching at this temperature immediately after hot rolling, is illustrated in figure 2.6c. Using EDS analysis, Knutsen detected partitioning of nickel to the austenite bands and chromium to the delta ferrite grains. On furnace cooling to room temperature, partial regression of some of the austenite to ferrite was observed (see figure 2.6d). Although the delta ferrite grains have recrystallised, the matched growth of several adjacent delta subgrains results in a continuous ferrite / martensite boundary. The directionality of the original δ / γ boundary is thus maintained. Knutsen found that the Ni and Cr content of the new ferrite is the same as that of the parent austenite. It would seem that partition of the substitutional alloying elements between the phases is not necessary, and that the reaction is controlled by the diffusion of the interstitial elements.

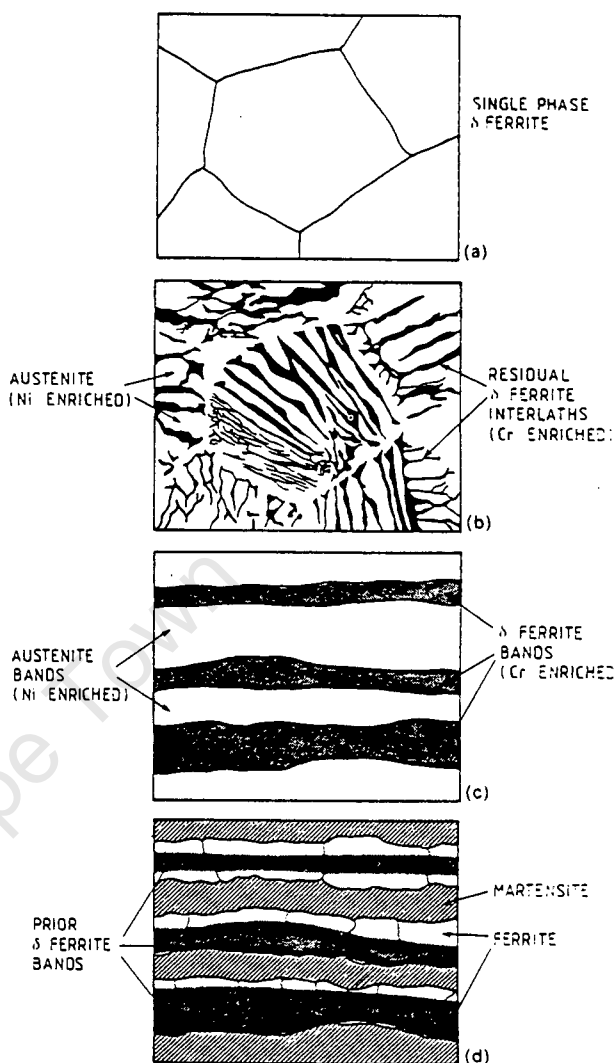


Figure 2.6 Evolution of the microstructure of 3CR12 (after reference 20).

2.1.3.3 Important Temperatures and Events During the $\gamma \rightarrow \alpha$ Transformation

Many of the experiments performed for this thesis involved the following procedure.

The alloy was: i) Heated to 1000°C in 2 hours

ii) Held at this temperature for 1 hour

iii) Continuously cooled to room temperature at 1°C / min.

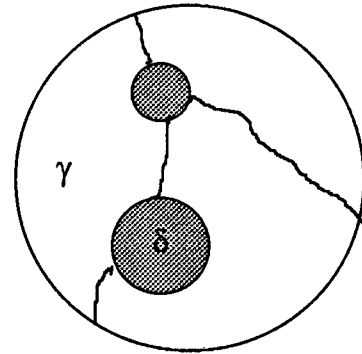
A proper understanding of the microstructural changes occurring during the latter part of this sequence is thus crucial, and a summary of the process based on the aforementioned literature is illustrated in figure 2.7 overleaf.

Temperature

Microstructure

1000°C

Phase equilibrium reached between austenite and δ -ferrite after 1 hour soak at 1000°C



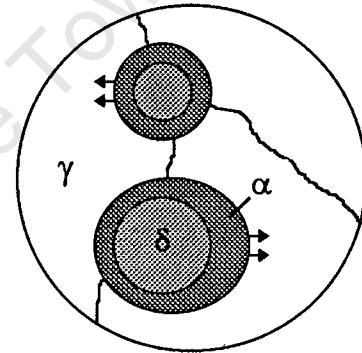
Non-equilibrium cooling between 1000°C and the Ar_3 temperature. Undercooling not yet sufficient for alpha ferrite nucleation.

Ar_3

Transformation begins



Alpha ferrite grows under non-equilibrium conditions



Ar_1

Transformation ends



M_s

Formation of martensite begins



M_f

Formation of martensite ends and final structure is present

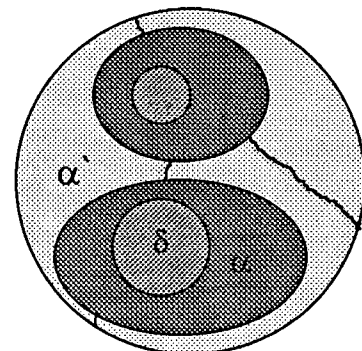


Figure 2.7 Important microstructural changes in 3CR12 during cooling from 1000°C.

2.2 EFFECTS OF ALLOYING ELEMENTS ON HIGH TEMPERATURE PHASE STABILITY

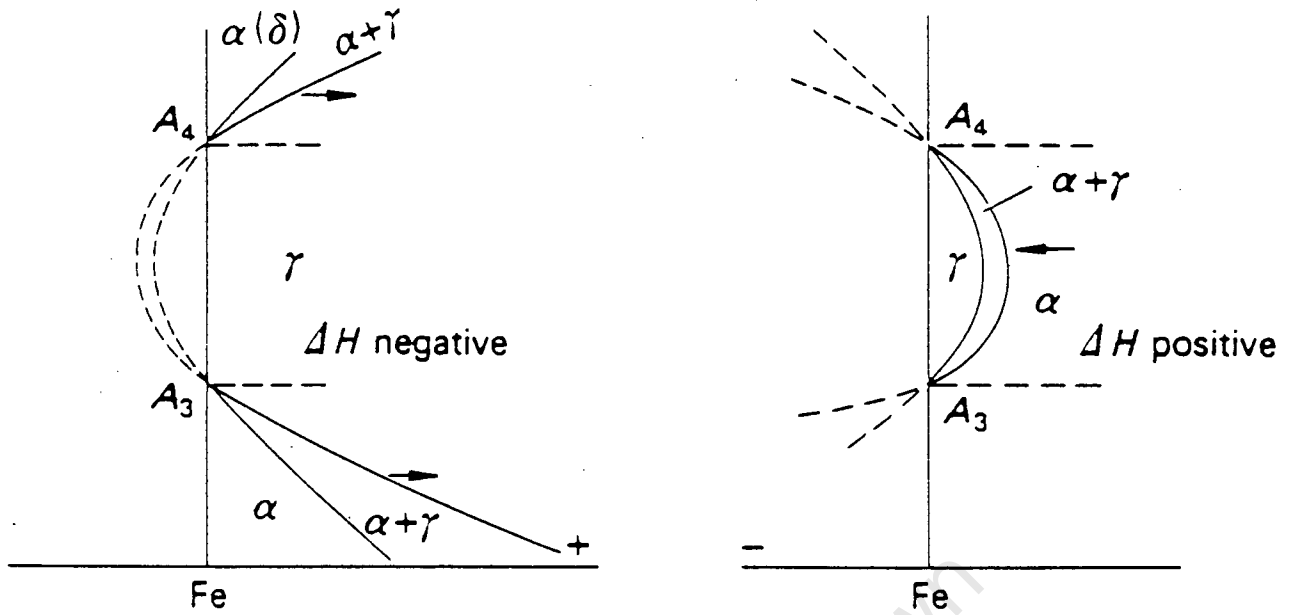
The presence of delta ferrite in 3CR12 during hot rolling has been identified as the key factor behind the anisotropic microstructure found after cooling. Alloying elements which decrease the quantity of this phase will have to be found. The alloying additions in steels have traditionally been divided into austenite and ferrite formers. Zener [23] developed a thermodynamic explanation for the austenite / ferrite stabilising effect of an element. If c_γ and c_α are the fractional concentrations of an element in the γ and α phases, the following relationship holds:

$$\log \frac{c_\alpha}{c_\gamma} = \frac{\Delta H}{RT}, \quad \Delta H = H_\gamma - H_\alpha$$

H_γ is the increase in enthalpy caused by the addition of one unit of the element to austenite, and similarly for H_α and ferrite. This treatment leads to two fundamental types of phase diagrams, one for austenite formers ($\Delta H < 0$) and one for ferrite formers ($\Delta H > 0$). They are illustrated over the page in figure 2.8. Histograms indicating which elements are austenite / ferrite formers, and their relative strengths, are shown in figure 2.9. The values of ΔH used in this analysis were found empirically, and no attempt was made to explain why an element had a particular value.

The interstitial elements, C and N, are seen to be by far the strongest of the austenite formers. However, since the attractive metallurgical properties of 3CR12 are due in part to the steel's low interstitial content, the content of these elements cannot be varied in order to obtain a higher austenite content.

The position of the element cobalt in this regard is somewhat uncertain. For various systems, it has been reported to be both a weak ferrite former [4, 24] and an austenite former [2, 3].



a) For γ stabiliser

b) For α stabiliser

Figure 2.8 The two fundamental types of phase diagrams, according to the theory of Zener (after reference 25).

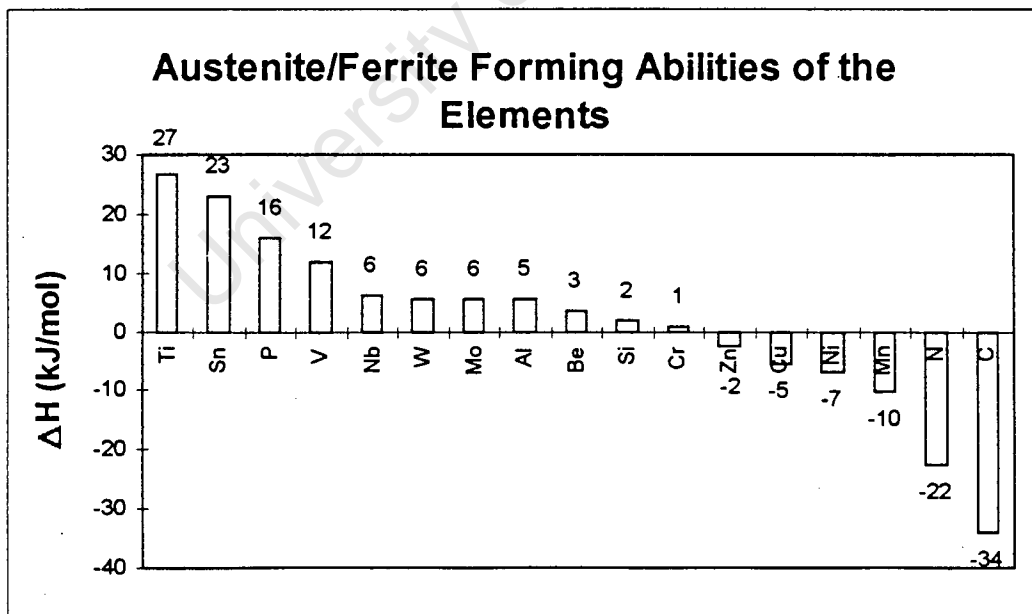


Figure 2.9 The relative strengths of the elements, according to the theory of Zener. For ferrite formers, $\Delta H > 0$.

2.2.1 High Temperature Delta Ferrite Content

Hewitt [4] performed an extensive investigation into the effect of various elements on the austenite / ferrite content of 3CR12 at 1000°C. Specimens were brought to equilibrium at this temperature and quenched, and the martensite content found by volume fraction analysis. The results are shown in table 2.2. The coefficient of each element represents the increase in the volume fraction of delta ferrite at 1000°C produced by the addition of 1 % of the element.

Table 2.2 The effect of alloying additions on the ferrite content of 3CR12 at 1000 °C.

Element	Effect	Element	Effect	Element	Effect
C	-290	Ti	+60	Nb	+45
S	+495	Co	+0,4	V	+13
P	+220	Mo	+2,0	N	-100
Mn	-6,2	Cr	+8,3	Zr	+110
Si	+32	Ni	-12,6	Ce	-1420
Cu	-24	Al	+12		

Irvine et al [3] studied the effects of alloying elements on the delta ferrite content of a 0,1% C - 15% Cr steel at 1050°C. Table 2.3 shows the effect of the addition of 1 % of each element on the ferrite content.

Table 2.3 Effect of elements on the ferrite content of a 0,1% C - 15% Cr steel at 1050 °C.

Element	Effect	Element	Effect	Element	Effect
N	-220	Cu	-7	Cr	+14
C	-210	Mn	-6	V	+18
Ni	-20	Si	+6	Al	+54
Co	-7	Mo	+5		

The results of the two authors are in broad agreement, although there are two interesting differences. Irvine found aluminium to be the strongest of the ferrite formers, whilst Hewitt determined it to be a mild austenite stabiliser. The allegiance of cobalt is again in doubt, with Hewitt finding it to have a virtually neutral effect, and Irvine finding it to be an austenite former of similar strength to Cu and Mn. This variance might be due to the different base compositions used in the studies.

Both authors cautioned that the results obtained may not be due to the thermodynamic effects of the elements alone. Carbide and nitride forming elements such as titanium and niobium, and to a lesser extent vanadium and aluminium, may increase their apparent stabilisation of ferrite by removing the austenite forming interstitials from solution.

For many years, much research has gone into the formulation of chromium and nickel equivalents for other alloying elements in stainless steels. Schaeffler [26] studied the structure of austenitic welds, and published the following equations, to be used in conjunction with a microstructure diagram:

$$\text{Cr equivalent} = \% \text{Cr} + 2,5(\% \text{Si}) + 1,8(\% \text{Mo}) + 2(\% \text{Nb})$$

$$\text{Ni equivalent} = \% \text{Ni} + 0,5(\% \text{Mn}) + 30(\% \text{C}).$$

Several other authors have determined their own equivalents to be used for specific steels. The results of many of these studies have been used in the formulation of the following generally accepted equations [27]:

$$\text{Cr equivalent} = \% \text{Cr} + 2(\% \text{Si}) + 1,5(\% \text{Mo}) + 5(\% \text{V}) + 5,5(\% \text{Al}) + 1,75(\% \text{Nb}) + 1,5(\% \text{Ti}) + 0,75(\% \text{W})$$

$$\text{Ni equivalent} = \% \text{Ni} + \% \text{Co} + 0,5(\% \text{Mn}) + 0,3(\% \text{Cu}) + 30(\% \text{C}) + 25(\% \text{N}).$$

2.2.2 Effects of the Elements on the A_{c1} Temperature

Hewitt [4] has performed an extensive study of the effects of alloying elements on the A_{c1} temperature of 3CR12, the results of which are summarised in table 2.4 below. The coefficient of an element represents the change in the A_{c1} temperature produced by the addition of 1 % of the element.

Table 2.4 The effect of the addition of an element on the A_{c1} temperature of 3CR12.

Element	Effect	Element	Effect	Element	Effect
C	-280	Ti	+83	Nb	+15
S	-100	Co	-21	V	+78
P	+435	Mo	+45	N	-230
Mn	-54	Cr	+13	Zr	+36
Si	+34	Ni	-70	Ce	+88
Cu	-23	Al	+40		

Irvine et al [3] studied the effects of alloying elements on the A_{c1} temperature of a 0,1% C-12% Cr steel. His results are summarised in table 2.5. The results of the two studies are in good agreement.

Table 2.5 The effect of the addition of 1 % of an element on the A_{c1} temperature of a 0,1% C-12% Cr steel.

Element	Effect	Element	Effect
Ni	-30	Al	+30
Mn	-25	Mo	+25
Co	-5	V	+25
		Si	+50

2.3 THE EFFECTS OF ALLOYING ELEMENTS ON THE TRANSFORMATION RATE

This section of the review is divided into two parts. The first part deals with the various ways in which substitutional alloying elements in general may affect the nucleation and growth kinetics of alpha ferrite in steels. Part two reports on various studies of the effects of particular elements.

2.3.1 How Alloying Elements Affect Nucleation and Growth Kinetics

There are at least six factors dependent on the addition of alloying elements which can be considered to affect the rate of nucleation and growth of alpha ferrite. Each of these in turn will now be discussed.

2.3.1.1 Thermodynamics

The driving force for the nucleation of any phase is the decrease in G , the Gibbs free energy, which may result. A significant factor in this energy decrease, ΔG , is the difference, ΔG_v , between the volume free energy of the parent phase and that of the new phase. For heterogeneous nucleation the critical radius, r^* , and the critical increase in free energy, ΔG^* , can be written as functions of ΔG_v , as follows [28]:

$$r^* = \frac{2I}{(\Delta G_v - \Delta G_s)}$$

$$\Delta G^* = \frac{16I^3\pi}{3(\Delta G_v + \Delta G_s)^2} S(\Theta)$$

Here ΔG_s is the strain energy attending nucleation, I is the energy per unit of interfacial area, and $S(\Theta)$ is a function of the wetting angle. Consider a quantity of austenite existing at a temperature below the Ae_3 , but before ferrite nucleation has begun (i.e. the undercooling ΔT is not large enough to overcome ΔG^* .) The addition of a ferrite

stabilising element will increase the free energy advantage of ferrite over austenite at a given temperature, and thus increase ΔG_v .

Figure 2.10 illustrates how this leads to a decrease in ΔG^* and r^* . The green line represents the contribution of the interfacial energy, which increases with r^2 . The thick blue line represents the volume free energy, and the thick red line the net energy change, prior to the addition of a ferrite stabilising element. The addition of a ferrite stabilising element leads to a reduction in the volume free energy curve (now the thin blue curve), which in turn leads to a reduction in r^* and ΔG^* (from the thin red curve).

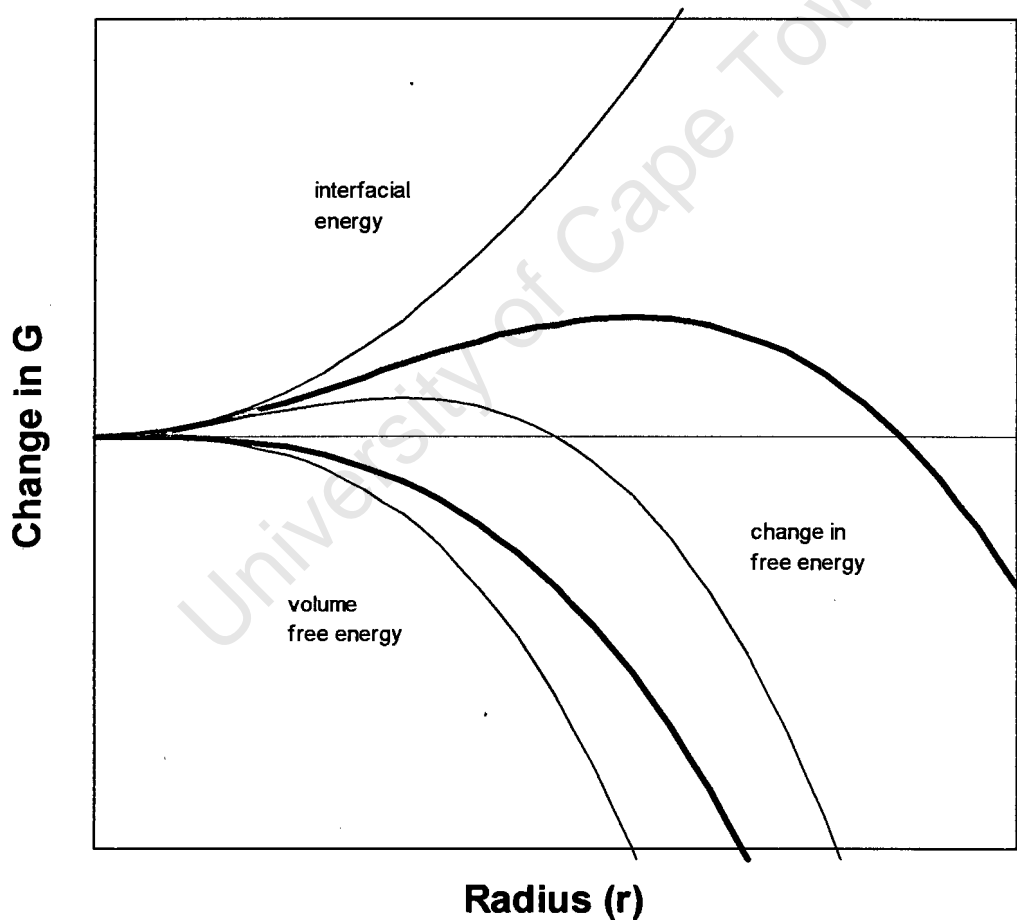


Figure 2.10 The free energy balance during heterogeneous nucleation.

2.3.1.2 Delta Ferrite Content

The delta ferrite content of 3CR12 at the soaking temperature has been found to influence the kinetics of the subsequent decomposition of austenite to alpha ferrite. Pistorius and Van Rooyen [29] investigated the continuous cooling transformation (CCT) behaviour of 100 alloys with compositions similar to that of 3CR12. The authors studied the effects of these elements, the A_{c1} temperature, and the austenite content at 1000°C, on the kinetics of the subsequent transformation. They defined a parameter, $\log(t_{50\%})$, which represents the time to cool to the ferrite start temperature at a rate which would result in the transformation of 50 % of the austenite to ferrite. Multiple regression analysis yielded an equation for $\log(t_{50\%})$ as a linear function of each of the elements, the A_{c1} temperature and the austenite content (f_γ). The coefficient of f_γ was given as 1,376, which indicates that a higher austenite content leads to higher values for $t_{50\%}$ and thus slower transformation kinetics. However, the authors made no attempt to explain this result.

Koepke et al [30] studied the transformation from 1000°C of three 0,07% C-13% Cr-0,2% Si-0,4% Mn steels containing additions of Ni and Mo. They found the nickel-rich alloy to contain the least delta ferrite, and the molybdenum-rich alloy to contain the most. The authors referred to previous studies which showed that the presence of delta ferrite in similar steels had dramatically reduced the incubation time for the formation of pearlite. This was thought to be because the presence of carbides at delta ferrite grain boundaries, and the boundaries themselves, provided favourable nucleation conditions for pearlite. In their study, the authors found that the nickel rich alloy did not contain visible amounts of delta ferrite, and transformation was initiated at austenite grain boundaries. In the other two alloys, pearlite nucleated at delta ferrite / austenite boundaries. Transformation to pearlite was able to occur at faster cooling rates in the alloys containing delta ferrite. Pearlite was observed to grow very rapidly close to the islands of ferrite, and to occur more slowly away from the delta ferrite.

2.3.1.3 Interphase Boundary Precipitation

Interphase boundary precipitation (IBP) occurs during the diffusional growth of ferrite from austenite and involves the formation of particles of a third phase at the γ / α interface. The third phase is often cementite [31] or alloy carbides [32], whilst on occasion the nucleation of pure metals has been observed [33]. The ferrite and the third phase do not grow co-operatively, as in the pearlitic reaction. There is as yet no theory correlating alloying elements and IBP.

Interphase precipitation is associated with both the step mechanism and continuous growth mode of ferrite growth [34]. In the former case, the carbides precipitate on the stationary component of the interface, because the steps themselves move too rapidly. The precipitates nucleate in contact with both the austenite and ferrite lattices, and adopt a crystallographic orientation which allows good matching with both of the phases.

In the latter case, pinning of the γ / α interface results. If the particles form random dispersions and are relatively coarsely spaced, the boundary migrates by bowing between them. If the precipitates are closely spaced, sometimes forming regular non-planar sheets, a “quasi-ledge” mechanism operates (see figure 2.11). The curved γ / α interface becomes pinned by the finely spaced particles. At a position where the particle spacing is relatively large, an interface bulge develops, and subsequently becomes pinned. It is, however, able to spread laterally, and a ledge mechanism of growth results.

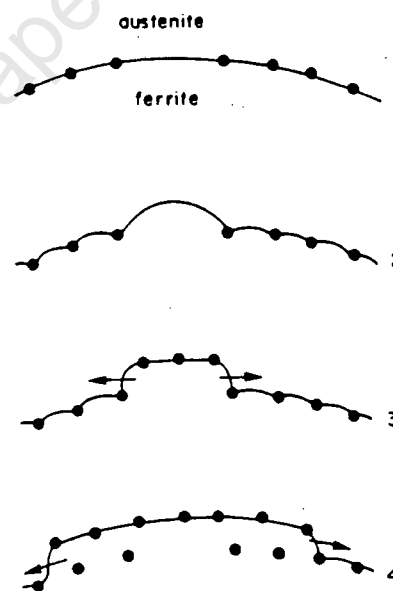


Figure 2.11 A schematic diagram showing the operation of a quasi-ledge mechanism of ferrite growth, as a result of α / γ interface pinning caused by IBP (after reference 34).

2.3.1.4 Solute Drag-Like Effect (SDLE)

Experiments in recrystallisation have convincingly demonstrated the existence of solute induced drag on grain boundary motion [34]. The effect is rationalised in terms of the segregation of solute atoms to moving grain boundaries. The solute-boundary interaction energy, G_s , is negative or positive, depending on whether there is adsorption or desorption of the impurity atoms. The solute can be dragged along with the boundary ($G_s < 0$), or pushed ahead of the boundary ($G_s > 0$), reducing the rate of migration relative to that in a pure material.

Conventional SDLE theories involve the transport of solute in the direction of boundary movement. So-called “special” solute drag effects have been proposed for cases where this atom motion is ruled out. Bradley and Aaronson [35] proposed such an effect in order to explain discrepancies between experimental and predicted ferrite growth rates. They hypothesized that atoms of alloying elements (X atoms) which differ appreciably in size to iron atoms, or which are markedly attracted to carbon atoms, or both, segregate to γ / α boundaries during growth. Such segregation is visualised as the “sweeping up” of X atoms, rather than the diffusion of X to these boundaries. If X significantly decreases the activity of carbon in austenite which is in contact with these boundaries, the carbon concentration in the austenite will be reduced, and so will the growth kinetics. Conversely, if X increases the activity of carbon in austenite and still segregates to γ / α boundaries because the resulting strain energy reduction overcomes the free energy increase associated with C-X repulsion, the carbon concentration gradient in austenite, and the growth kinetics of the boundaries, will be increased. This is referred to as an inverse SDLE [36].

Table 2.6 Qualitative guide to the effects of elements on the activity of carbon.

Element	Effect	Element	Effect
Si	increase	Mn	decrease
Ni	increase	Cr	decrease
Co	increase		

2.3.1.5 Partition of Alloying Elements During Growth

The solubility of a substitutional alloying element in ferrite and austenite will generally be significantly different, with a ferrite stabilising element having, of course, a higher solubility in that phase. If the transformation is allowed to proceed under equilibrium conditions, partition of the element between the two phases will occur. There are three different models for the partition of elements between austenite and ferrite during the (isothermal) growth of ferrite [35]. These are:

i. Partition under local equilibrium (P-LE)

Full equilibrium is maintained, with bulk partition of carbon and the alloying elements (see figure 2.12a).

ii. Negligible partition under local equilibrium (NP-LE)

Local equilibrium is maintained at the boundary, but with bulk partition of C only. The alloying elements maintain local equilibrium by “piling up” at the boundary (see figure 2.12b).

iii. Paraequilibrium

Local equilibrium is not maintained at the boundary, since only carbon partitions. There is no movement of substitutional alloying elements (see figure 2.12c).

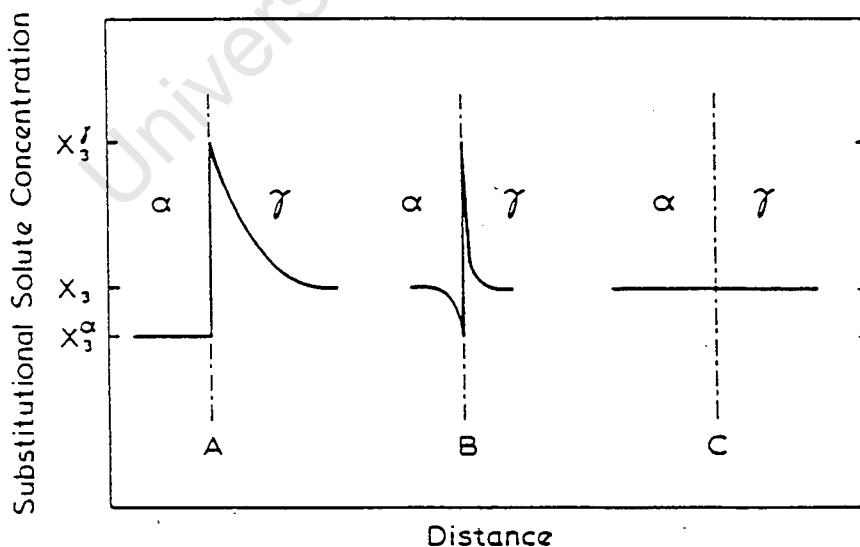


Figure 2.12 Three modes of element partition in steel (after reference 35).

At low alloying element supersaturations, an γ / α interface may migrate with sufficient partition to maintain full equilibrium [37]. Growth is then controlled by diffusion of these elements. At higher supersaturations, growth may occur by the NP-LE mode. This requires minimal diffusion of the alloying elements, and is controlled by the diffusion of carbon. Alternatively, growth may occur by paraequilibrium, which is also controlled by diffusion of carbon. Since the diffusion rate of substitutional alloying elements in ferrite or austenite is about five orders of magnitude less than that of interstitial elements [25], growth under conditions of full equilibrium can be expected to be significantly slower than when carbon alone undergoes bulk partition.

2.3.1.6 Elevation of the Reaction Temperature

As discussed in section 2.2.2, alloying elements may change the A_1 and A_3 temperatures of a steel. Ferrite stabilising elements will increase the range of stability of this phase and therefore raise these temperatures. The growth of ferrite from austenite is dependent on the diffusion of iron and carbon atoms, and sometimes of substitutional alloying elements. Since diffusion coefficients increase with temperature according to the Arrhenius equation [38], an elevation of the transformation temperature range will increase the kinetics of ferrite formation. Austenite forming elements will have the converse effect of a decrease in the A_1 and A_3 temperatures and slower rates of ferrite growth.

In the study by Pistorius and Van Rooyen [29] referred to in section 2.3.1.2, the effect of the A_{c1} temperature on the kinetics of the transformation of 3CR12 were also studied. In the equation derived for $\log(t_{50\%})$, the coefficient of A_{c1} is given as -6.252×10^{-3} . As expected, a higher A_{c1} temperature leads to a lower value for $\log(t_{50\%})$ and accelerates the reaction.

2.3.2 The Effect of Specific Alloying Elements on the Transformation Rate

This section reviews studies where the effect of specific elements on the transformation kinetics has been determined. Most of this work has been performed on low alloy steels, although at least one study on 12 % Cr steel has been performed.

2.3.2.1 The Transformation Kinetics of 12 % Cr Steels

Pistorius and Van Rooyen [29] studied the continuous cooling transformability of 3CR12-type steels with additions of a number of alloying elements. They published an equation for the time to the onset of transformation at the cooling rate which resulted in 50 % ferrite formation. Their relationship is based on a model derived by Mostert and Van Rooyen [39] for low alloy steels, which used CCT diagrams from international databases. The equation considers the effects of many elements, includes an interaction coefficient for titanium and the interstitials, as well as factors for the Ac_1 temperature (see section 2.3.1.6) and the austenite volume fraction at the soaking temperature of 1000°C (see section 2.3.1.2). Ti and Si were the only elements found to encourage the transformation.

Table 2.6 The co-efficients of the elements required to calculate $\log(t_{50\%})$ (t in seconds) according to the equation derived by Pistorius and Van Rooyen.

Element	Effect	Element	Effect
constant	6,346	Nb	3,366
Mn	1,115	B	128,3
Si	-0,9552	(C+N)	10,61
Ti	-7,958	Ti \times log(C+N)	-5,302
Mo	0,8275	f_γ	1,376
Cr	0,1686	Ac_1 (°C)	$-6,252 \times 10^{-3}$
Ni	1,608		

2.3.2.2 Growth Kinetics in Low Alloy Steels

Most investigations into the kinetics of ferrite growth have been performed on low alloy steels, and some of these will now be discussed. However, it must be borne in mind that these results cannot simply be extrapolated to alloys with different compositions. In addition, most of these studies involve the *isothermal* decomposition of austenite.

Aaronson and Domian [37] obtained data for the Time-Temperature-Transformation (TTT) curves for 0,1 and 0,4 wt % C high purity steels, as well as for a range of such steels containing individual additions of one of Si, Mn, Ni, Mo, Co, Al, Cr and Cu. They found that Si, Al and in some cases Co displaced the TTT curve for the initiation of transformation of ferrite grain boundary allotriomorphs to shorter times, whilst Mo, Cr, Cu, Ni and Mn adjusted it to longer times. The relative effect of aluminium was found to be greater than that of silicon.

They used electron microprobe analysis to investigate the partition of alloying elements between austenite and newly formed ferrite at isothermal transformation temperatures between 400 and 1000°C. No partition was found in the Si, Al, Mo, Co, Al, Cr and Cu steels. In the Mn, Ni and Pt alloys, partition occurred above an individually characteristic critical temperature. The critical temperature was 130, 65 and 35°C below the Ae_3 for Mn, Ni and Pt respectively. For isothermal decomposition

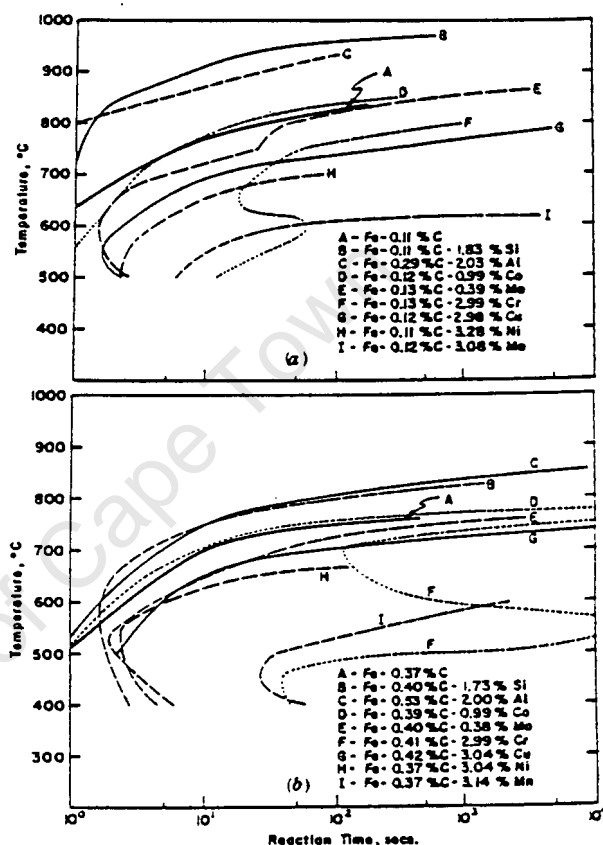


Figure 2.13 TTT curves for the initiation of transformation in Fe-C and Fe-C-X alloys (after reference 37).

treatments in this temperature range, the time to initiation of transformation was significantly longer (see figure 2.13).

In an accompanying paper, Aaronson, Domian and Pound [40] attempted to explain these results using thermodynamic theories of ferrite nucleation and growth. They studied the decrease in Gibbs free energy, ΔG , on transformation from austenite to ferrite. They showed that Mn, Ni and Cu lessen ΔG , with Mn having the most notable effect. Co, Si and Al all increase ΔG , and thus should encourage the growth of ferrite.

Kinsman and Aaronson [41] performed a similar study upon the kinetics of ferrite allotriomorph growth in Fe-C-X alloys containing Si, Al and Co. The authors noted that these three elements are unlikely to exert a solute-drag type of effect because they either increase or slightly decrease the activity of carbon in austenite. They found that all three elements displace the TTT curves for the initiation of transformation to shorter times (see figure 2.14). The parabolic rate constant, α , for allotriomorph thickening was calculated, and it was found that Al and Si increase α , whilst Co had little if any effect. The volume free energy change associated with nucleation, ΔG_v^n , was also calculated for each alloy (see figure 2.15). All three elements were found to increase this parameter, with Al and Si being significantly more effective than Co. The authors attributed the increased reaction rates to an increase in driving force.

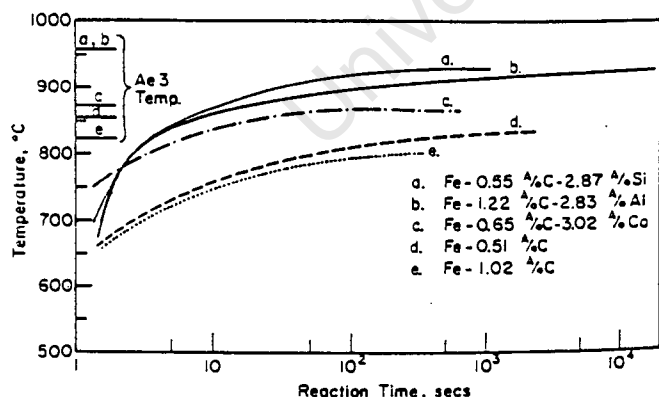


Fig. 1—TTT curves for the beginning of transformation for the five alloys studied.

Figure 2.14 The TTT curves for the initiation of transformation. (After reference 41.)

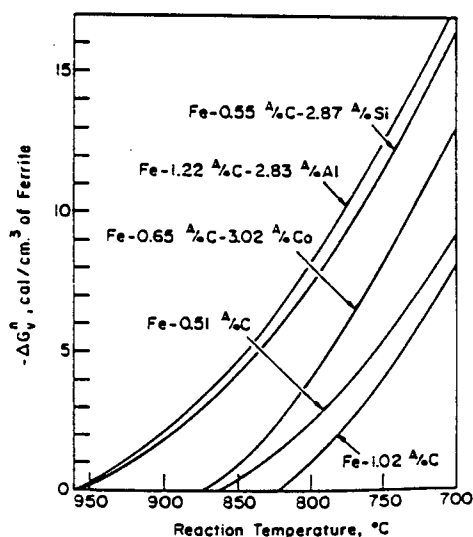


Figure 2.15 The effect of the elements on ΔG_v^n . (After reference 41.)

Bradley and Aaronson [35] investigated the isothermal thickening and lengthening in Fe-C-X alloys, where X = Si, Ni, Mn and Cr. The purpose of this study was not to ascertain the effectiveness of the elements in enhancing the transformation, but to compare theoretical predictions with experimental results. Several of their explanations for anomalous predictions are of interest. The first is interphase boundary precipitation, which may pin ferrite / austenite boundaries and cause the transformation to be slower than expected. In an accompanying paper, a TEM study performed by Shiflet et al [36] found interphase boundary precipitation to have occurred in the Si and Ni alloys, which had transformed faster than predicted. The authors hypothesized that the growth kinetics had been accelerated by the consequent increase in the carbon concentration gradient caused by the removal of carbon. This is the opposite effect to that normally expected from IBP. Ni and Si increase the activity of carbon in austenite and thus an inverse solute drag-like effect might contribute to the faster than expected growth kinetics.

More recently, Tanaka et al [24] investigated the growth kinetics of grain boundary ferrite allotriomorphs in Fe-C-Mn- X_2 alloys, where X_2 was successively Si, Ni and Co. In all cases the parabolic thickening rate constant, α , was significantly less than in Fe-C- X_2 alloys previously investigated. The Fe-C-Mn-Ni alloy had considerably slower growth kinetics than Fe-C-Mn, whilst the addition of Si increased the growth rate slightly at a specific temperature. The addition of cobalt did not have a noticeable effect. The inhibiting effect of manganese, which is known to reduce the activity of carbon in austenite, was ascribed to a solute drag-like effect.

3. EXPERIMENTAL MATERIALS AND METHODS

3.1 EXPERIMENTAL MATERIALS

3.1.1 Alloy Compositions

The following composition, modelled on that of 3CR12, was selected for the base alloy:

C	N	Cr	Mn	Si	Ni
0,02	0,02	12	1	0,35	0,35

The effects of Si and Ni were investigated by increasing the amounts included, and additions of Cu, Co and Al were made. The additions of these five elements to the alloys studied in this thesis are shown below.

Table 3.1 The compositions of the alloys used in this work, excluding the constant composition of 0,02 % C, 0,02 % N, 12 % Cr and 1 % Mn. (Note that all compositions are in wt %, unless otherwise stated.)

Alloy no.	Alloying Elements				
	Co	Cu	Ni	Si	Al
Base	0,01	0,06	0,41	0,34	0,005
1	0,97	0,07	0,34	0,33	0,001
2	1,53	0,07	0,35	0,33	0,001
3	0,02	1,50	0,34	0,41	0,006
4	0,02	1,53	0,33	0,99	0,002
5	1,57	1,53	0,35	0,33	0,001
6	1,58	1,51	0,35	0,94	0,001
7	1,58	1,54	0,35	0,33	0,093
8	1,58	1,52	0,35	0,92	0,054
9	0,01	0,06	0,94	0,33	0,006
10	0,01	0,06	0,95	0,34	0,151
11	0,01	0,06	0,94	1,03	0,104

It was hoped that the addition of Cu, and an increase in the Ni content, would result in a significant expansion of the austenite field, and that Si and Al would encourage the decomposition of austenite. However, it was feared that the elements would have a negative effect as well, with Cu and Ni slowing the transformation, and Si and Al stabilising ferrite. The inclusion of cobalt was made with the idea that it might stabilise austenite *and* encourage the transformation to ferrite, a seemingly contradictory effect.

3.1.2 Production Route

The alloys were produced at the Columbus Laboratory in Middelberg. They were cast into moulds which can hold up to 7 kg of steel, and which produce ingots of 37-38 mm thickness. Split heats were produced from 20kg melts in order to maintain constant Cr, Mn and interstitial levels. All heats were individually analysed in order to check these levels. Immediately after casting, the steels were hot charged into a silicon carbide heating element reheat furnace and soaked for an hour at 1250°C. They were then put through a multipass rolling schedule, with about 25% reduction per pass. Total rolling time was about 1 minute and the final thickness about 9 mm. Last pass temperature was between 950 and 1000°C, after which the plates were air cooled.

3.2 EXPERIMENTAL PROCEDURES

3.2.1 Dilatometry

The dilatometer used for this thesis was previously constructed in the department using some parts from an older production model. For the purposes of this thesis, the dilatometer was modified in order to increase the heating and cooling rates which it could handle. A quartz furnace tube, which has excellent thermal shock resistance and a low thermal mass, was used instead of an alumina tube. A new furnace chamber was constructed to accommodate a silicon carbide crucilite tube element, which can withstand very rapid heating and cooling rates.

Data capture from the dilatometer was performed as follows. The voltages from a thermocouple (the tip of which was touching the specimen) and a linear variable differential transformer were processed by computer hardware and then converted to values of temperature and extension by a computer program.

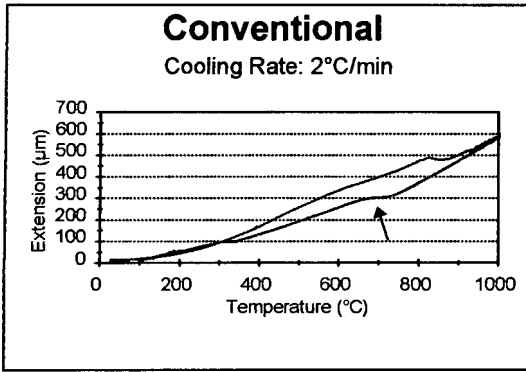
The dilatometer was used for two purposes: to obtain critical cooling rates for the initiation of transformation, and to find transformation start and finish temperatures. The methods used for this are now discussed in detail.

3.2.1.1 Determination of Critical Cooling Rates

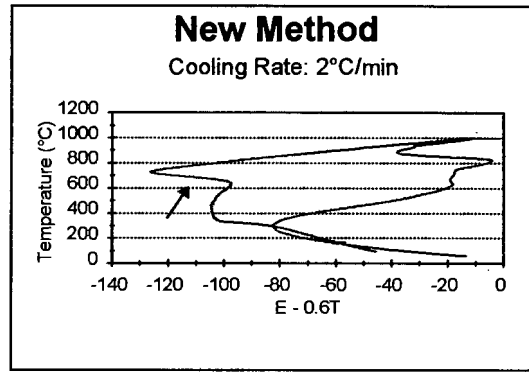
Dilatometry was used to find the critical cooling rate for each alloy for a fully untransformed structure. The procedure was to heat a specimen of the alloy to 1000°C in two hours, soak for an hour to reach phase equilibrium, and then to cool at a specified rate. The extension (E) vs temperature (T) graph was then studied, and the next cooling rate selected. The absence of an inflection point in the normal transformation range was initially taken to indicate a fully untransformed structure. However, volume fraction analysis of a specimen cooled at this rate showed the presence of 15 % alpha ferrite. A more sensitive gauge of an untransformed structure was needed.

This extra sensitivity can be obtained by a method used at Columbus Laboratory, whereby a variation of the conventional E vs T graph is plotted. Temperature is plotted as a function of the quantity $E - \lambda T$, where λ is a constant. The effect of this is to make the "effective expansion coefficient" of the ferrite 0 (instead of $12 \times 10^{-6} \text{ K}^{-1}$), which allows for amplification of the austenite "effective expansion coefficient". A value for λ of 0,6 was found to be most effective in reducing the effective expansion of ferrite.

Figure 3.1a overleaf shows a conventional E vs T graph of alloy 8 heated to 1000°C and then transformed at 2°C/min. Part b shows the same data, but plotted using the new method. The cooling section of the curve is on the left hand side of the graph. Both these graphs indicate that an intermediate amount of transformation to alpha ferrite has taken place (arrowed). Figure 3.1c shows the standard graph for alloy 8

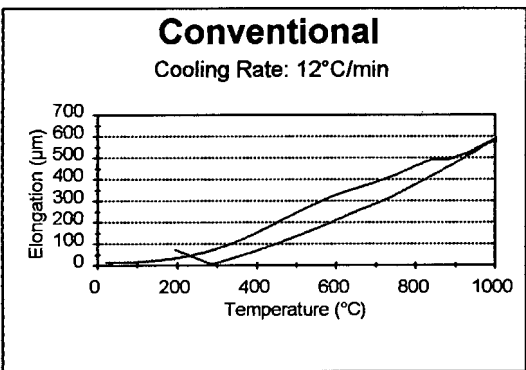


a)

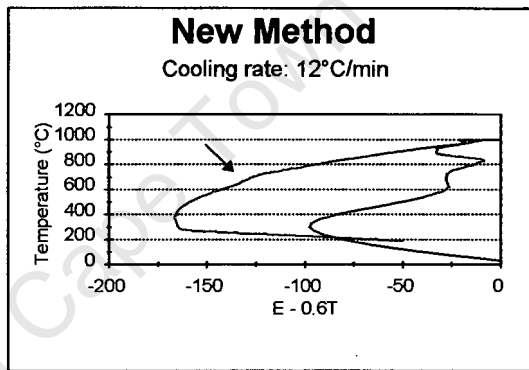


b)

Both methods indicate an intermediate amount of transformation at 2°C/min

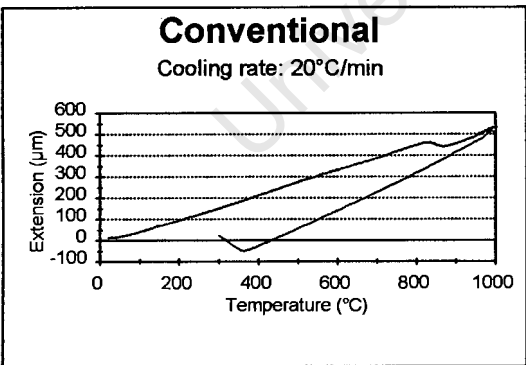


c)

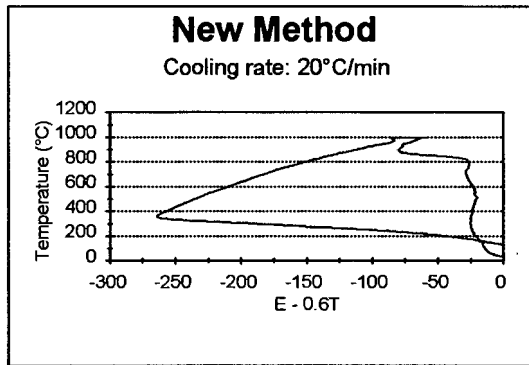


d)

Only the new method shows an inflection point at 12°C/min



e)



f)

Neither method shows an inflection point at 20°C/min.

Figure 3.1 This figure shows dilatometry graphs of alloy 8 cooled at 3 different cooling rates, each plotted in both the conventional manner and using the new method. At 12°C/min, only the new method exhibits an inflection point in the transformation range. (Some of the data has been smoothed.)

cooled at 12°C/min. The absence of an inflection point in the transformation range would have indicated a fully untransformed structure. However, examination of the same data plotted using the new method (figure 3.1d) shows a definite inflection point in this range (arrowed). Figures 3.1e and f show the conventional and T vs E - λT graphs for alloy 8 cooled at 20°C/min. The E vs T graph again shows no point of inflection. However, figure f also shows an absence of an inflection point, and alloy 8 is considered "fully untransformed". The slowest cooling rate at which a point of inflection is not observed is taken as the critical cooling rate for a fully untransformed structure. Volume fraction analysis of a specimen cooled at this rate shows the presence of 4 % alpha ferrite, which is the accepted limit of resolution for this work.

3.2.1.2 Determination of Transformation Temperatures

If the dilatometer graph is linear either side of the transformation range, then the upper and lower transformation points, the A_3 and A_1 respectively, can be defined as the temperatures where the curve deviates from linearity [42]. This was found to be the case for the alloys studied in this thesis, and a computer programmer was commissioned to write software which would perform this procedure. The program requires the input of two temperatures, one below the A_1 , and the other above the A_3 . The best fit straight line from the given temperature to the nonlinear region of the graph is then found, and the transformation point defined as where the curve deviates significantly from the straight line. An illustration of the performance of the program is shown in figure 3.2 overleaf.

Determination of Transformation Temperatures

Alloy 10: Heated at 0,5°C/min

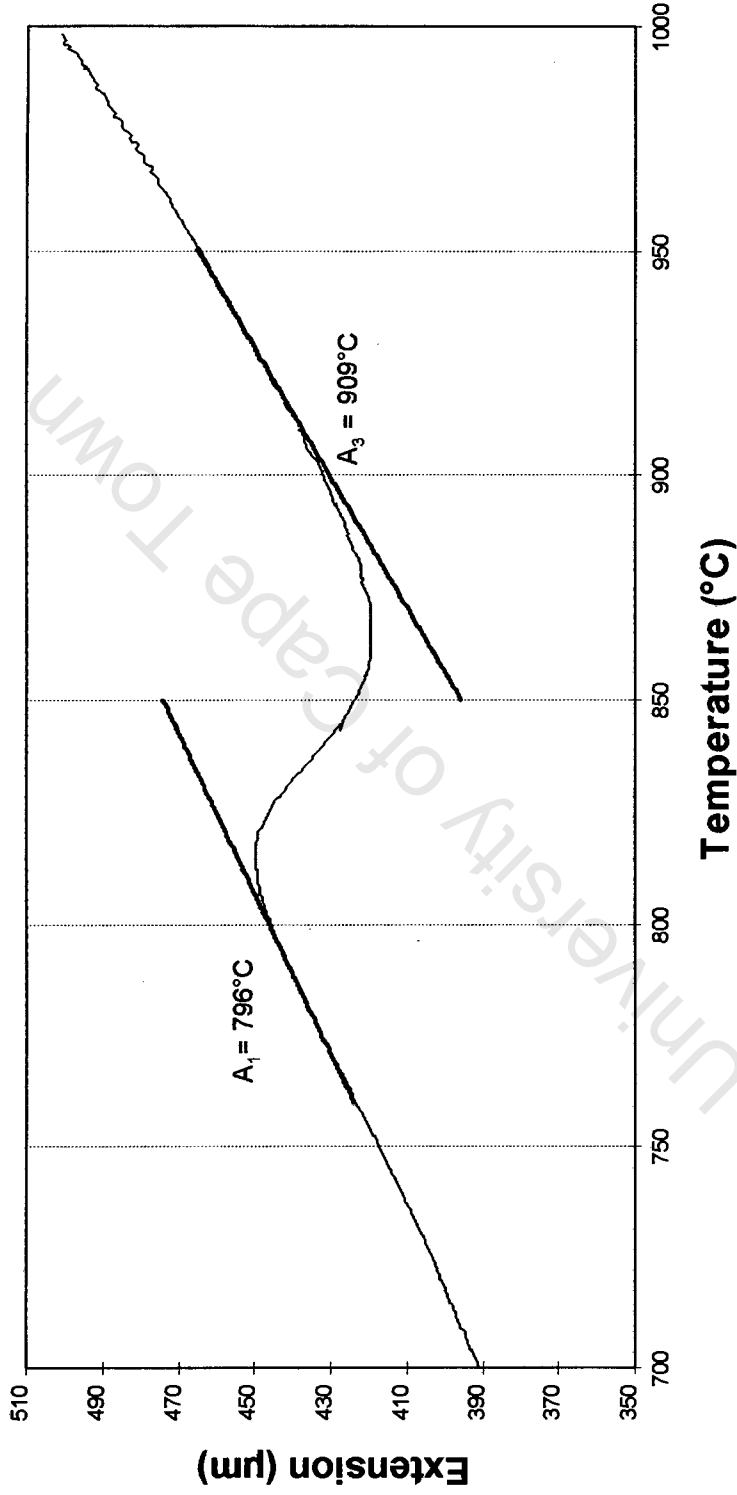


Figure 3.2 The transformation points of the alloys are found by fitting straight lines to the linear sections of the curves and finding the points where the deviation becomes significant.

3.2.2 Metallography

3.2.2.1 Optical Microscopy

Specimens were cut, mounted and polished using conventional metallurgical techniques. In all cases, the through thickness-rolling direction face of the sample was studied. The final surface finish was obtained by a mechanical polish with a 0,25 μ m diamond paste. For most specimens, a colour etchant recommended by Beraha and Shpigler [43] was used. The composition of the etchant is as follows:

3g potassium metabisulfite
1,5g sulfamic acid
0,75g ammonium bifluoride (= ammonium hydrogen difluoride)
100ml distilled water

The etchant reacts with the specimen and the reaction product is deposited on the surface. It acts as a thin interference film and causes differential colouration which can be microscopically resolved. The etching time was 30-35 seconds, and immediately afterwards the specimens were rinsed in warm water and then placed in a beaker of alcohol in an ultrasound bath.

An electrolytic etchant, with composition given below, was used for volume fraction analysis specimens quenched from 1000°C.

25g chromium trioxide
133ml acetic acid
7ml distilled water

This formula gives excellent contrast between delta-ferrite and martensite when viewed using interference contrast. Specimens were first electropolished at 20V for 1-2 minutes. They were then electroetched in the same solution, using a current of a 0,025 A/cm² for about two minutes.

Specimens were analysed using a REICHERT MeF3A optical microscope. Nomarski interference contrast was used for imaging the electroetched specimens.

3.2.2.2 Transmission Electron Microscopy (TEM)

Specimens for TEM studies were taken from the same samples as used for optical microscopy. Slices of thickness 1mm were cut from the same face as the light microscope specimens. They were then ground down to a thickness of 200-300 μ m on silicon carbide abrasive paper. A mechanical punch was used to obtain discs 3mm in diameter. The discs were then ground on abrasive paper to a thickness of 50-80 μ m. Thinning was carried out using a STRUERS Tenupol-3 electrolytic polishing unit. A solution of 5% perchloric acid in methanol was used at a potential difference of 35V and at a temperature of -15°C. The microscope used was a JOEL 200CX operating at 200 kV.

3.2.3 Volume Fraction Analysis (VFA)

The analysis was performed by point counting, which is regarded as the most accurate and efficient manual method [44, 45]. The optical microscope was linked to a colour monitor using a video camera. Adhesive tape of width 1mm was used to construct a grid on the screen of the monitor. Eleven horizontal lines and ten vertical lines were drawn using this tape, with the intersections of these lines providing the points of the grid. Magnification levels were used such that, as far as possible only one grid point fell on a given particle of interest [46]. If a point fell on the boundary between two phases, it was counted as a ½ for each phase. One hundred fields of view were counted for each specimen which was analysed. The points lying in the phase with the smaller volume fraction were counted. The average number of points in this phase over 100 fields of view was calculated, and divided by 110 (the number of grid intersections) to obtain the volume fraction. The fraction of the second phase was found by subtraction.

The uncertainty in the VFA results was determined using a method described by Underwood [47]. The percentage accuracy (%acc) is given by the following equation:

$$\%acc = \frac{200s}{\sqrt{Nm}}$$

where s is the population standard deviation, N the number of grids counted, and m the mean number of points per grid.

3.2.4 Compositional Analysis

3.2.4.1 Electron Microprobe Analysis

A CAMECA Camebax Microbeam electron microprobe (EMP) was used to obtain line scans of elemental composition on specimens prepared for optical microscopy. The initial point of the line was selected using an attached optical microscope, after which the number of counts of each element for a period of 10 seconds was recorded using a wavelength dispersive spectrometer. The probe was then moved a distance of several μm to the next point to be analysed. The length of the line analysed was 30 - 50 μm . The spatial resolution of the EMP for this work is about 3 μm .

3.2.4.2 Scanning Electron Microscopy

The light microscope specimens were also studied using a CAMBRIDGE S200 scanning electron microscope (SEM) with a TRACOR Northern TN5400 energy dispersive X-ray microanalyser. This instrument was primarily used to investigate the compositions of particles precipitated at grain boundaries and within grains. Due to the small size of the particles, the X-ray interaction volume could be expected to include a portion of the matrix. In order to enable an approximate allowance for the matrix contribution to be made, spectra were obtained for the matrix as well. The inclusion spectra were then processed by subtracting the matrix spectrum from the inclusion spectra after normalisation with respect to the iron $K\alpha$ peak. In view of the limited accuracy of this method, no effort was made to quantitatively analyse the spectra. In addition, carbon and nitrogen, which would be expected to be present, cannot be detected by EDS.

3.2.5 Laboratory Hot Rolling

Specimens of length 65 mm (in the rolling direction) and width 60 mm were cut from the rolled, air cooled plates. Prior to deformation, the samples were soaked in a furnace at 1000°C to obtain phase equilibrium. They were then put through a sequence of five double passes, being reduced by about 0,8 mm each time, for a total reduction of about 40%. Between each double pass, the specimen was returned to the furnace and brought back to the soaking temperature. After the last pass, the sample was placed in a second furnace at the A_{r3} temperature and cooled to room temperature.

3.2.6 Mechanical Properties

3.2.6.1 Impact Testing

Toughness testing was performed at room temperature using an AVERY impact tester. Substandard Charpy V specimens with dimensions 55×10×3,3mm were machined from the plates hot rolled in the laboratory. For each alloy, 4 specimens were milled in the T-L orientation, and 4 in the L-T orientation (see figure 2.3). The initial energy of the pendulum was 165 J.

3.2.6.2 Tensile Testing

Tensile testing was carried out using a ZWICK universal tester equipped with a 200 kN load cell. Conventional Hounsfield metric specimens with a gauge length of 25,2 mm and gauge diameter of 5,04 mm were machined with the tensile axis in the rolling direction. The specimens were subcritically annealed at 725°C for 2 hours before being strained at room temperature at a rate of 10^{-3} /sec. Three specimens were tested for each result.

4. EXPERIMENTAL RESULTS

4.1 ASPECTS OF THE $\gamma \rightarrow \alpha$ TRANSFORMATION

This section investigates several aspects of the decomposition of austenite to ferrite in 3CR12. Firstly, the mode of formation of alpha ferrite, by epitaxial growth from delta ferrite / austenite interphase boundaries, has been confirmed using a combination of optical and transmission electron microscopy. Secondly, the effect of increasing the delta ferrite content at 1000°C on the anisotropy of the fully transformed microstructure is discussed. Thirdly, two factors which may affect the rate of the transformation are discussed. These are:

- Precipitation during cooling from 1000°C
- Element partition during transformation.

4.1.1 Epitaxial Growth

A combination of optical and transmission electron microscopy was used to study the epitaxial growth of alpha ferrite from delta ferrite during the decomposition of austenite in 3CR12. A specimen of alloy 8 was soaked for an hour at 1000°C and then cooled to room temperature at 1°C/min. The optical micrograph shown in figure 4.1a on page 44 demonstrates that the microstructure consists of elongated delta ferrite bands (white) surrounded by alpha ferrite grains. The absence of grain boundaries between the two types of ferrite is the telltale sign of epitaxial growth.

This observation is confirmed by the TEM micrograph of the same specimen shown in figure 4.1b. The double line of precipitates corresponds to the similar stringers in the optical micrograph. The delta ferrite band, which has recrystallised into several grains, extends to just before the fine array of precipitates. Some dislocations can also be observed. Once again, no boundary between the two types of ferrite can be seen, indicating that epitaxial growth has occurred.

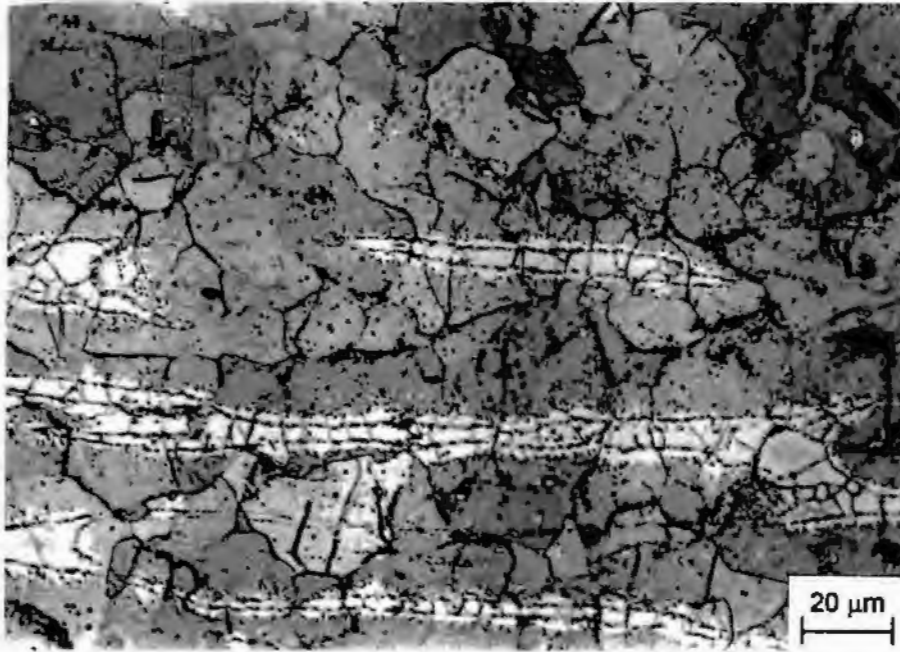


Figure 4.1a Optical micrograph of the complete decomposition of austenite to alpha ferrite (grey) by epitaxial growth from elongated delta ferrite (white) grains.

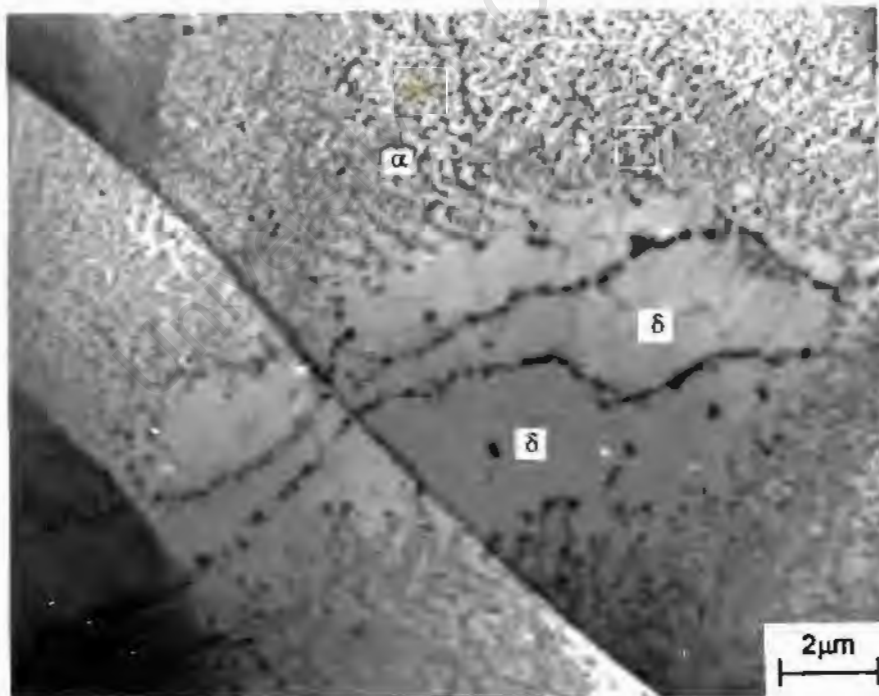


Figure 4.1b TEM micrograph of the epitaxial growth of alpha ferrite from a recrystallised delta band.

4.1.2 Delta Ferrite Content and the Resulting Microstructural Anisotropy

Knutsen [20] has shown that the presence of delta ferrite in 3CR12 during hot rolling leads to the formation of an anisotropic microstructure on cooling. The deformation leads to the soft ferrite phase becoming highly elongated in the rolling direction. On cooling, the austenite transforms to alpha ferrite by epitaxial growth of the delta ferrite into the surrounding austenite. The result is the retention of the anisotropic delta ferrite grain morphology.

This picture is complicated by the dynamic recrystallisation of the delta ferrite grains during hot deformation. Epitaxial growth of alpha ferrite grains takes place individually from the recrystallised grains of the delta ferrite stringers, leading at least one author [11] to report the presence of an equiaxed structure in 3CR12 after cooling. However, several sources of anisotropy remain.

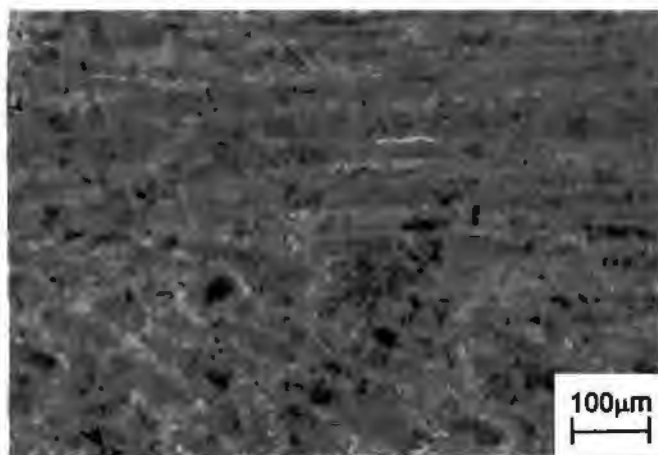
Firstly, the “boundaries” between delta ferrite and adjacent alpha ferrite grains remain elongated in the rolling direction. Although these are not true grain boundaries, the matching between the alpha ferrite and delta ferrite lattices will not be perfect due to their different compositions (see section 4.2.3). In addition, the presence of aligned precipitates at or close to these borders will contribute to their susceptibility to crack propagation.

Secondly, alpha ferrite grains migrating from adjacent grains of a delta ferrite band appear to grow at the same rate [20]. When the temperature becomes too low for diffusion and growth stops, an elongated boundary is formed between these alpha grains and the martensite laths which form on further cooling.

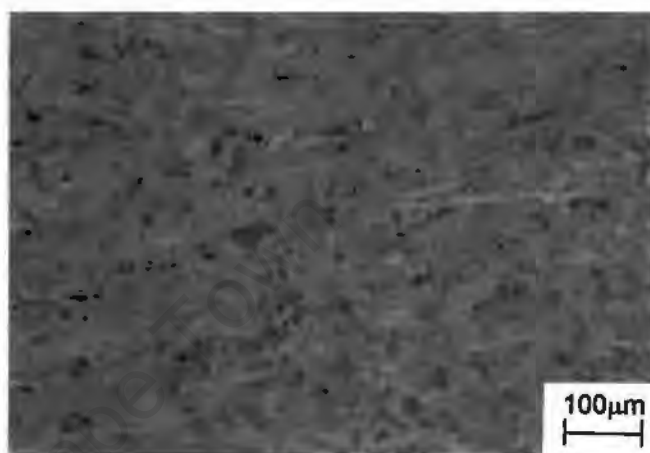
In figure 4.1, the effect of increasing the delta ferrite content on the resulting microstructural anisotropy is illustrated. The structures of alloys 7 and 4 are shown after two heat treatments. The alloys have firstly been soaked for an hour at 1000°C and quenched. The micrographs of these specimens (figure 4.2a) show that the delta ferrite grains have retained the elongated morphology produced during the rolling of the heats at the Columbus mill. The larger volume fraction of delta ferrite in alloy 4

(14,9 % compared to 2,2 % for alloy 7) has resulted in this alloy having a more severely anisotropic structure at 1000°C.

In the second treatment the alloys were allowed to cool to room temperature at 1°C/min, instead of being quenched. The micrographs (figure 4.2b) show that the difference in anisotropy at 1000°C has been carried through to room temperature.

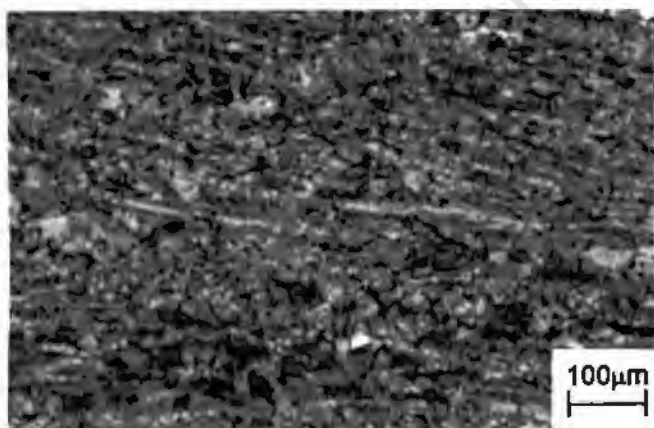


Alloy 7



Alloy 4

Figure 4.2a The structures of the alloys at 1000°C, consisting of elongated δ -ferrite grains (white) in a martensitic (austenite at temperature) matrix. (Colour etchant.)



Alloy 7



Alloy 4

Figure 4.2b After cooling at 1°C/min, the alloys are almost fully transformed, but the anisotropy, more prominent in alloy 4, remains. (Colour etchant.)

4.1.3 Precipitation During Cooling From 1000°C

The SEM was used to investigate precipitation in alloys 4, 6 and 8. In specimens soaked at 1000°C and then cooled at 1°C/min, two types of precipitation were observed. The first is the growth of large particles within delta ferrite grains, sometimes stringered parallel to grain boundaries. These particles were not present in specimens quenched from 1000°C. The second is the precipitation of finer particles in the newly formed alpha ferrite. Interestingly, both these types of precipitation were found only in the specimens containing Cu. Although the second type of precipitation occurs during the growth of alpha ferrite, it is not clear from the limited results of this study whether interphase boundary precipitation has occurred. However, the removal of carbon from solution caused by the formation of carbide particles might enhance the transformation kinetics by making carbon diffusion in austenite ahead of the advancing interface less necessary. Figure 4.3 shows SEM micrographs illustrating precipitation in alloys 4 and 6. Figure 4.1 on page 44 nicely illustrates this precipitation in alloy 8.

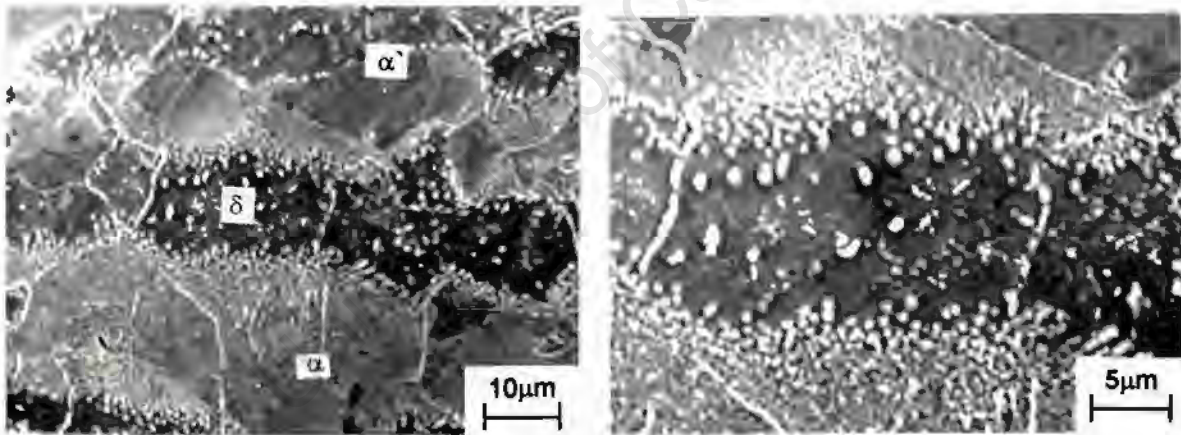


Figure 4.3a Precipitation in alloy 4, at low and high magnifications.

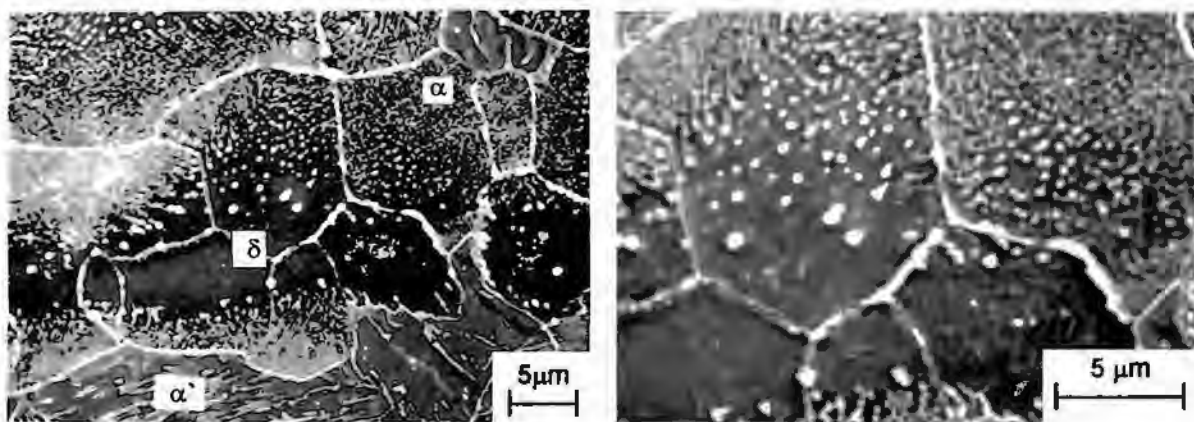


Figure 4.3b Precipitation in alloy 6, at low and high magnifications.

The compositions of the particles were analysed using energy dispersive spectroscopy (EDS), which does not measure C and N content. The particles of the first type were found to contain Cu, S, Si and Cr, and in the case of alloy 8, Al. The second type consisted largely of Cu and S, and sometimes Al in alloy 8. A sample of the spectra obtained using EDS are shown below.

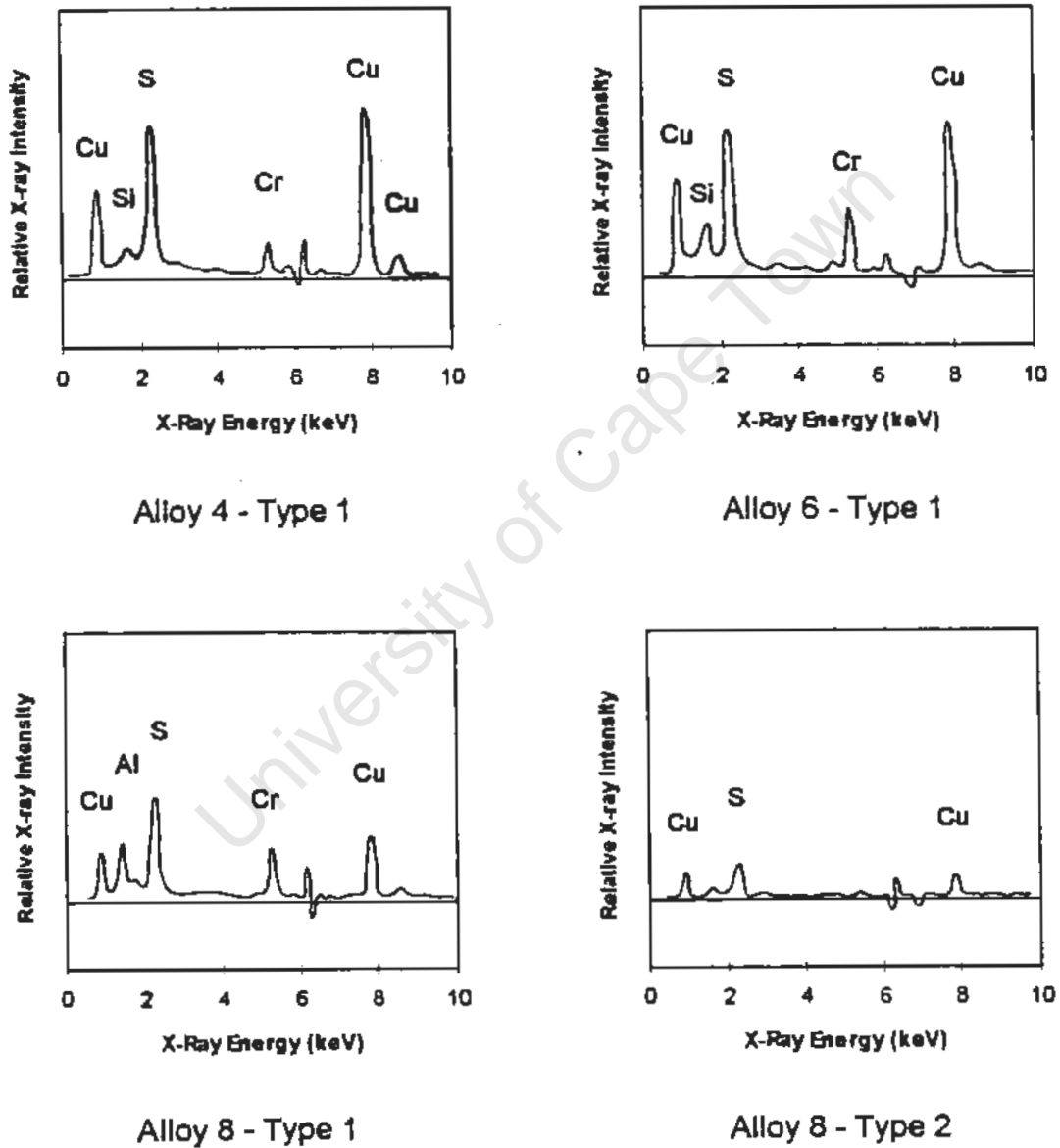


Figure 4.4 EDS analyses of the composition of precipitates in alloys 4, 6 and 8.

4.1.4 Element Partition During Transformation

Element partition was investigated by compositional microanalysis using an electron microprobe (EMP). A line scan was begun in a delta ferrite grain, continued through an alpha ferrite crystal and ended in a martensite (austenite at temperature) grain. The results for alloy 6 are shown in figure 4.5 below. There is no evidence for the partition of substitutional alloying elements between alpha ferrite and austenite during the transformation. There is evidence for partition of elements between delta ferrite and the other two phases. In section 4.2.3, this partition is shown to occur prior to the decomposition of austenite. These results were confirmed for alloy 4. The absence of partition of substitutional elements during the transformation indicates that bulk diffusion of only the interstitial elements is necessary during the transformation.

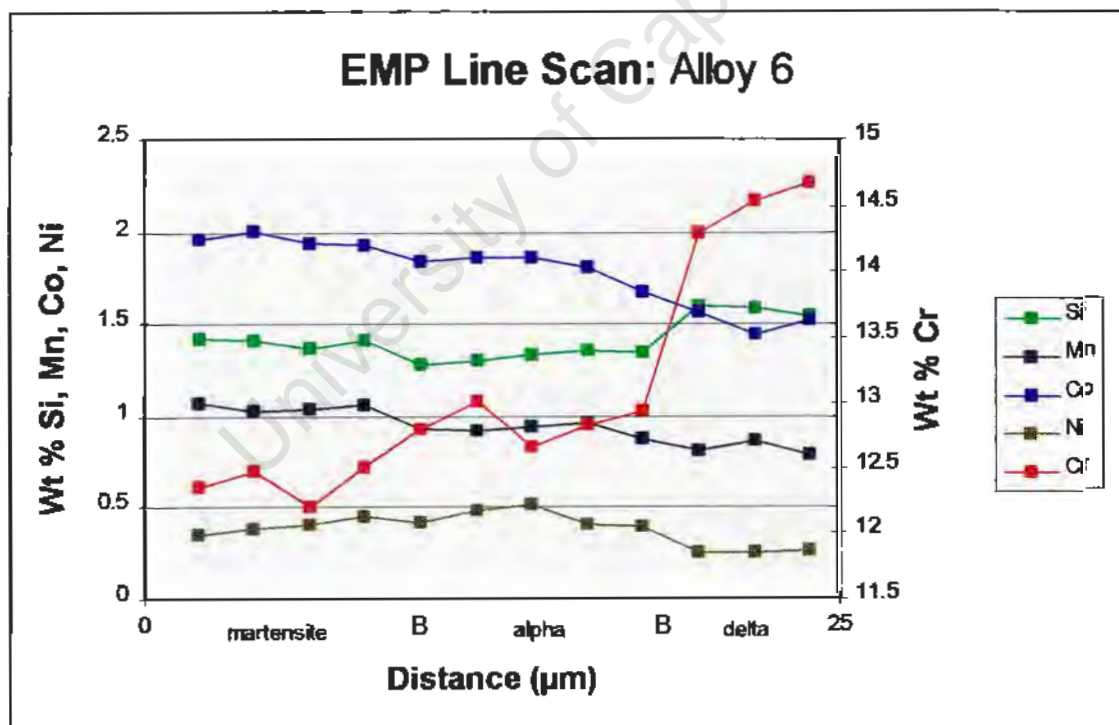


Figure 4.5 An EMP line scan of alloy 6 shows an absence of element partition during the transformation to alpha ferrite. The letter B indicates a grain boundary.

4.2 ALLOYING ELEMENTS AND HIGH TEMPERATURE PHASE STABILITY

Three methods were used to investigate the effects of the alloying elements on the austenite / ferrite phase balance. These are:

- Volume fraction analysis to find the phase content at 1000°C
- Dilatometry to obtain the A_{e1} and A_{e3} temperatures
- EMP analysis to study element partition between delta ferrite and austenite.

4.2.1 Delta Ferrite / Austenite Content at 1000°C

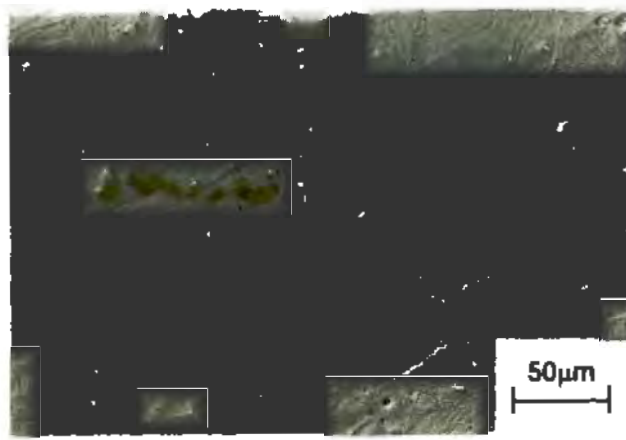
Specimens of each alloy were held at 1000°C for an hour and then oil quenched. Volume fraction analysis yielded the following results:

Table 4.1 Delta ferrite content of the alloys at 1000°C

Alloy no.	Alloying Elements					Percentage δ -ferrite
	Co	Cu	Ni	Si	Al	
Base	0,01	0,06	0,41	0,34	0,005	6,6 \pm 0,7
1	0,97	0,07	0,34	0,33	0,001	2,4 \pm 0,2
2	1,53	0,07	0,35	0,33	0,001	0,34 \pm 0,07
3	0,02	1,50	0,34	0,41	0,006	2,3 \pm 0,2
4	0,02	1,53	0,33	0,99	0,002	14,9 \pm 0,6
5	1,57	1,53	0,35	0,35	0,001	0,19 \pm 0,05
6	1,58	1,51	0,35	0,94	0,001	0,8 \pm 0,1
7	1,58	1,54	0,35	0,33	0,093	2,2 \pm 0,2
8	1,58	1,52	0,35	0,92	0,054	6,3 \pm 0,6
9	0,01	0,06	0,94	0,33	0,006	3,1 \pm 0,4
10	0,01	0,06	0,95	0,34	0,151	12,9 \pm 0,7
11	0,01	0,06	0,94	1,03	0,104	35 \pm 1

Comparing alloys 3, 4 and 9 to the base alloy, it can immediately be seen that cobalt, copper and nickel are acting as austenite stabilisers. Comparison of alloy 3 with 4, and alloy 9 with 10, shows that silicon and aluminium are having the opposite effect and act as ferrite formers.

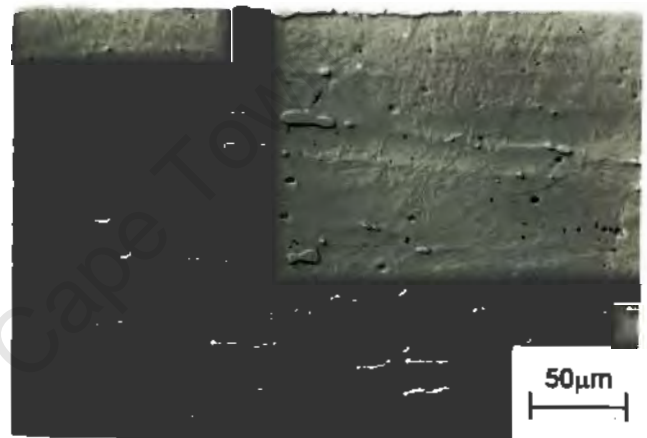
Optical micrographs of some of these specimens are shown in figures 4.6 and 4.7, and illustrate the effects of the elements on the delta ferrite content.



Alloy 2 - base + 1,5% Co - : 0,34% δ -ferrite



Base Alloy: 6,6% δ -ferrite

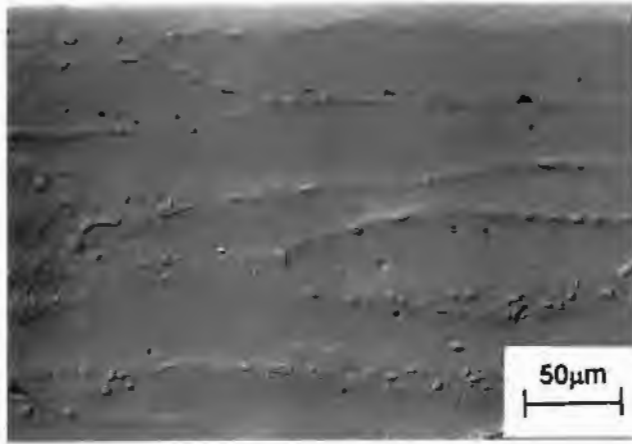


Alloy 3 - base + 1,5% Cu - : 2,3% δ -ferrite



Alloy 9 - base + 1% Ni - : 3,1% δ -ferrite

Figure 4.6 Equilibrium structures of the base alloy and alloys 2, 3 and 9 at 1000°C, showing the decrease in the volume fraction of delta ferrite caused by the austenite forming elements Co, Cu and Ni respectively. (Electrolytic etchant.)



Alloy 9 - base + 1% Ni - : 3,1% δ -ferrite



Alloy 10 - alloy 9 + 0,15% Al - : 12,9 % δ -ferrite



Alloy 11 - alloy 10 + 1% Si - : 35% δ -ferrite

Figure 4.7 Equilibrium structures of alloys 9, 10 and 11 at 1000°C, showing the increase in the volume fraction of delta ferrite due to successive additions of 0,15% aluminium and 1% Si. (Electrolytic etchant.)

4.2.2 The Ae_1 and Ae_3 Temperatures of the Alloys

The equilibrium transformation temperatures of the alloys were found using dilatometry (see section 3.2.1.2). A heating curve is regarded as being more accurate for this purpose than a cooling one, since the transformation takes place at higher temperatures and the diffusion required for equilibrium transformation can occur more easily. However, it is accepted that the the true transformation temperatures will be overestimated [48]. Specimens were heated at $0,5^{\circ}\text{C} / \text{min}$, the slowest heating rate which time constraints would allow, and the results are shown in the table below.

Table 4.2 The Ae_1 and Ae_3 temperatures of the alloys.

Alloy no.	Alloying Elements					Ae_1 ($^{\circ}\text{C}$)	Ae_3 ($^{\circ}\text{C}$)
	Co	Cu	Ni	Si	Al		
Base	0,01	0,06	0,41	0,34	0,005	810	914
1	0,97	0,07	0,34	0,33	0,001	799	877
2	1,53	0,07	0,35	0,33	0,001	795	869
3	0,02	1,50	0,34	0,41	0,006	784	871
4	0,02	1,53	0,33	0,99	0,002	800	888
5	1,57	1,53	0,35	0,33	0,001	752	834
6	1,58	1,51	0,35	0,94	0,001	785	869
7	1,58	1,54	0,35	0,33	0,093	771	849
8	1,58	1,52	0,35	0,92	0,054	797	879
9	0,01	0,06	0,94	0,33	0,006	772	871
10	0,01	0,06	0,95	0,34	0,151	795	909
11	0,01	0,06	0,94	1,03	0,104	837	914

Additions of copper and nickel led to a considerable reduction in both transformation temperatures, whilst cobalt has a slightly less dramatic effect. The temperature range over which austenite is stable is thereby increased, as expected.

Comparison of, for example, alloys 5 and 6, and alloys 5 and 7, show that silicon and aluminium are acting as ferrite formers and raising the equilibrium transformation temperatures.

4.2.3 Partition of Alloying Elements at 1000°C

The composition of adjacent delta ferrite and martensite (austenite at temperature) grains was studied using the electron microprobe (EMP). The same specimens used for VFA in section 4.2.1 (quenched from 1000°C after an hour soak) were examined in this work. The line scan was begun in a martensite region, traversed across a neighbouring ferrite grain, and continued into a second martensitic region. The composition was analysed every 2 to 3 microns over a range of about 40 μm . The results are shown in figure 4.8 on page 55. Figure 4.8a shows that Si and Cr are partitioning to delta ferrite, and Mn and Ni are favouring austenite. Figure 4.8b confirms these results for the ferrite formers, and indicates that Co and Cu are partitioning to austenite.

University of Cape Town

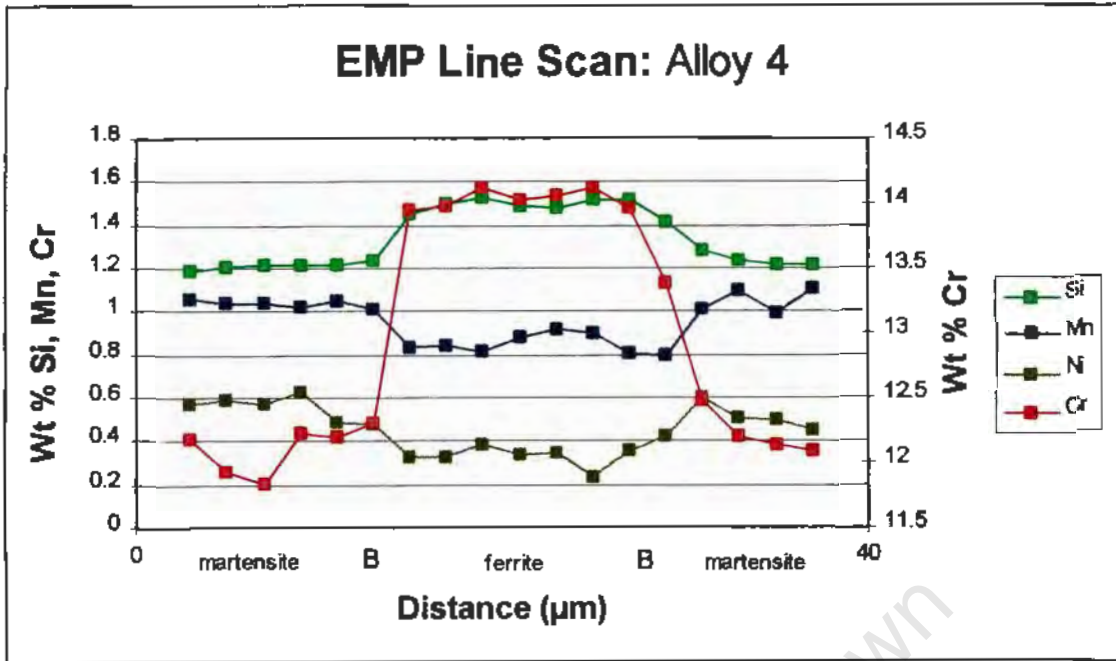


Figure 4.8a EMP line scan of alloy 4, showing partition of Si and Cr to ferrite, and Mn and Ni to austenite (now martensite).

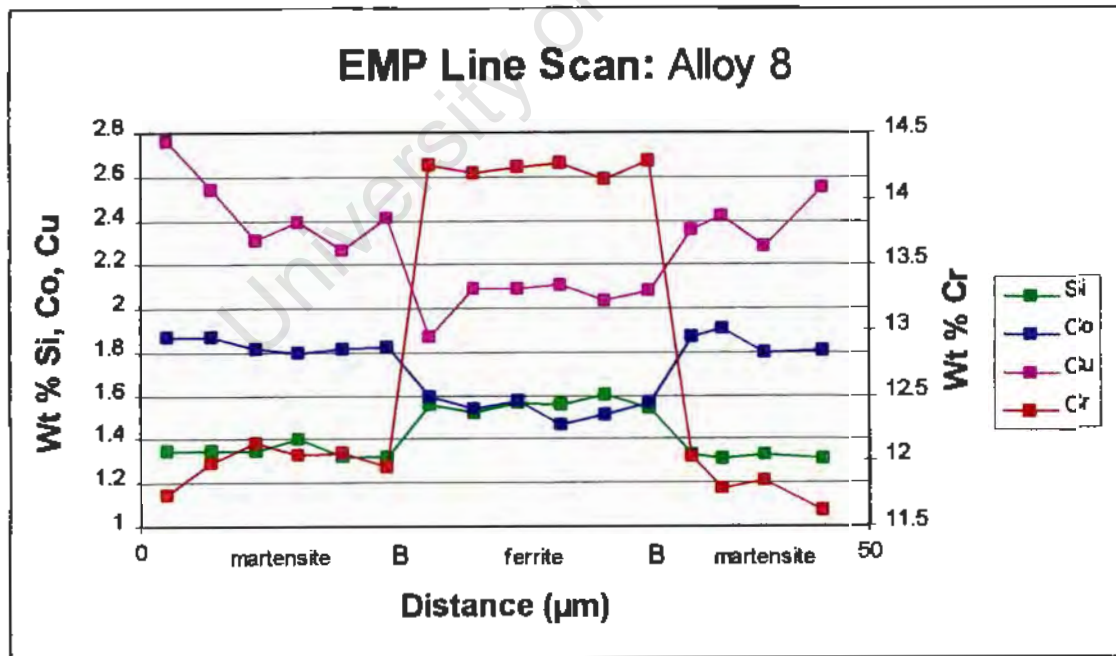


Figure 4.8b EMP line scan of alloy 8, showing partition of Si and Cr to ferrite, and Co and Cu to austenite (now martensite).

4.3 ALLOYING ELEMENTS AND THE RATE OF TRANSFORMATION

Two methods were used to quantify the speed with which the austenite to ferrite transformation occurred in the alloys. The first approach involves VFA and incorporates the results of section 4.2.1. The second method uses dilatometry to obtain the cooling rate for the growth of a 0,04 volume fraction of alpha ferrite.

4.3.1 Extent of Decomposition of Austenite After Cooling at 1°C / min

A specimen of each alloy was soaked at 1000°C for an hour to obtain an equilibrium structure, and then cooled to room temperature at 1°C/min. The proportions of ferrite (delta + alpha) and martensite present were then determined by VFA. Since the fractions of austenite and ferrite stable at 1000°C are already known from section 4.2.1, the amount of austenite which was able to transform to ferrite at the specified cooling rate could be calculated. The results are shown in table 4.3 below.

Table 4.3 The amount of ferrite which has been able to transform from austenite at 1°C / min, found by subtracting the martensite content after cooling from the austenite present at 1000 °C.

Alloy no.	Alloying Elements					% γ at 1000°C	% α' on cooling	% alpha formed
	Co	Cu	Ni	Si	Al			
Base	0,01	0,06	0,41	0,34	0,005	93,4	32	61 ± 2
1	0,97	0,07	0,34	0,33	0,001	97,6	45	53 ± 1
2	1,53	0,07	0,35	0,33	0,001	99,66	96,4	3,3 ± 0,4
3	0,02	1,50	0,34	0,41	0,006	97,7	84	13 ± 1
4	0,02	1,53	0,33	0,99	0,002	85,1	7,1	78 ± 1
5	1,57	1,53	0,35	0,33	0,001	99,81	99,81	0 ± 0,05
6	1,58	1,51	0,35	0,94	0,001	99,2	87	12 ± 1
7	1,58	1,54	0,35	0,33	0,093	97,8	0,8	97,0 ± 0,3
8	1,58	1,52	0,35	0,92	0,054	93,7	0	93,7 ± 0,6
9	0,01	0,06	0,94	0,33	0,006	96,9	93,6	3,3 ± 0,8
10	0,01	0,06	0,95	0,34	0,151	87,1	0	87,1 ± 0,7
11	0,01	0,06	0,94	1,03	0,104	65	0	65 ± 1

This method of estimating the transformation speed has an intrinsic limitation. If an alloy is fully transformed at a given cooling rate, there is no way of comparing its transformability with another fully transformed alloy. In the same way, its transformation speed cannot be compared with complete accuracy to an alloy which has undergone intermediate transformation. A similar restriction applies to alloys which are fully untransformed. These results are illustrated in figures 4.9, 4.10 and 4.11 on pages 58-60.

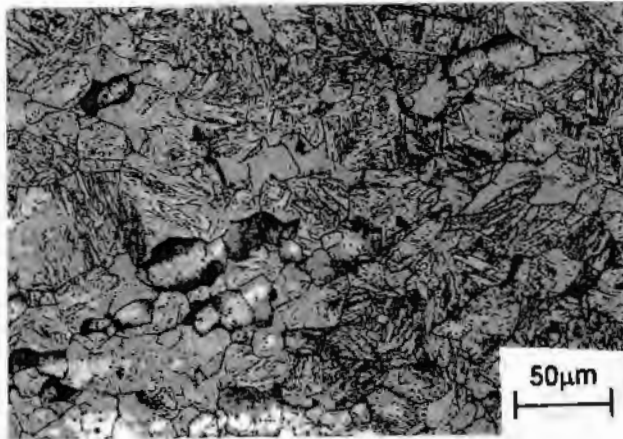
The temperature range over which the transformation takes place has been shown to influence the kinetics (see section 2.3.1.6). For this reason, the Ar_1 and Ar_3 temperatures of the alloys at a cooling rate of $1^\circ\text{C} / \text{min}$ were determined using dilatometry. Due to the limited amount of transformation occurring in some of the alloys, accurate values for the transformation temperatures could not be obtained from conventional dilatometric graphs. The data was therefore plotted using the new method discussed in section 3.2.1.1, but even then accurate values could only be obtained for 9 of the alloys.

Table 4.4 The transformation temperatures of some of the alloys, at $1^\circ\text{C}/\text{min}$.

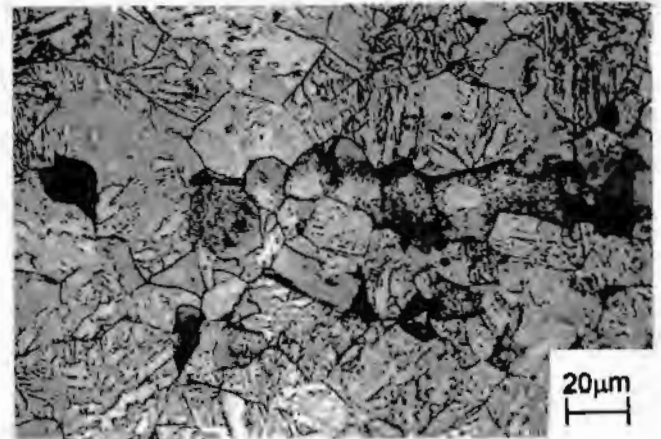
Alloy no.	Alloying Elements					Ar_1 ($^\circ\text{C}$)	Ar_3 ($^\circ\text{C}$)
	Co	Cu	Ni	Si	Al		
Base	0,01	0,06	0,41	0,34	0,005	645	793
1	0,97	0,07	0,34	0,33	0,001	586	773
3	0,02	1,50	0,34	0,41	0,006	600	754
4	0,02	1,53	0,33	0,99	0,002	591	734
6	1,58	1,52	0,35	0,94	0,001	591	734
7	1,58	1,54	0,35	0,33	0,093	595	733
8	1,58	1,52	0,35	0,92	0,054	674	769
10	0,01	0,06	0,95	0,34	0,151	590	782
11	0,01	0,06	0,94	1,03	0,104	631	830

Comparison of alloys 1 and 3 to the base shows that cobalt and copper significantly lower the transformation temperatures, whilst comparison of alloys 6 and 8 indicates that aluminium strongly increases them. The effects of silicon and nickel are not immediately clear from the limited number of results.

Alloy 6: 12% transformation at 1°C / min



Low Magnification

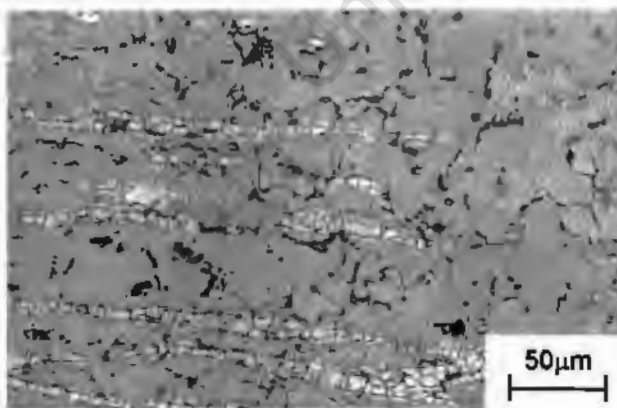


High Magnification

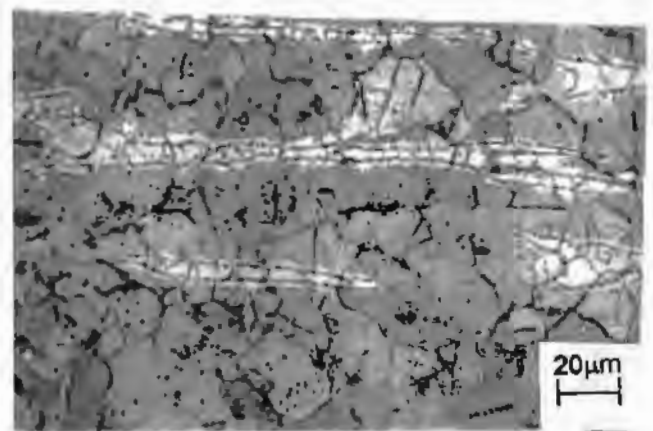
Delta ferrite (white) surrounded by alpha ferrite (grey), the rest martensite.

{ ADDITION OF 0,05% Al }

Alloy 8: 94% transformation at 1°C / min



Low magnification



High magnification

Delta ferrite (white) surrounded by alpha ferrite (grey).

Figure 4.11 The effect of the addition of 0,05% aluminium on the rate of transformation of alloy 6 after 1 hour soak at 1000°C. (Colour etchant.)

4.3.2 Critical Cooling Rates for the Initiation of Transformation

Dilatometry was used to find the slowest cooling rate for each alloy at which no inflection point appeared in the transformation range on the dilatometer curve, plotted using the new method (see section 3.2.1.1). These cooling rates were shown to correspond to about 4 % transformation to alpha ferrite. The results are shown in table 4.5 below.

Table 4.5 The critical cooling rates for the initiation of transformation.

Alloy no.	Alloying Elements					Cooling Rate (°C/min)
	Co	Cu	Ni	Si	Al	
Base	0,01	0,06	0,41	0,34	0,005	27
1	0,97	0,07	0,34	0,33	0,001	6
2	1,53	0,07	0,35	0,33	0,001	1,5
3	0,02	1,50	0,34	0,41	0,006	3
4	0,02	1,53	0,33	0,99	0,002	14
5	1,57	1,53	0,35	0,33	0,001	0,2
6	1,58	1,51	0,35	0,94	0,001	4
7	1,58	1,54	0,35	0,33	0,093	8
8	1,58	1,52	0,35	0,92	0,054	15
9	0,01	0,06	0,94	0,33	0,006	0,7
10	0,01	0,06	0,95	0,34	0,151	35
11	0,01	0,06	0,94	1,03	0,104	40

Additions of Co, Cu and Ni can be seen to lead to lower cooling rates, with nickel having the strongest effect. Comparing alloys 6 and 7 to alloy 5, Si and Al appear to enhance the transformation, although only alloys 10 and 11 have higher transformation rates than the base alloy. Aluminium is significantly more effective in enhancing the kinetics of the transformation than silicon.

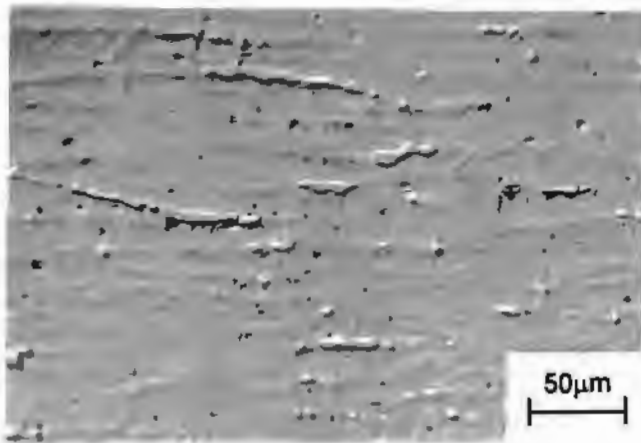
4.3.3 The Effect of Initial Ferrite Content on the Transformation Rate

Pistorius and Van Rooyen [29] suggested that increasing the amount of delta ferrite present at the soaking temperature would encourage the decomposition of austenite to alpha ferrite. Careful comparison of the values in the right hand column of tables 4.3 and 4.1 lends support to this idea, and figure 5.2 in section 5.2.3.1 illustrates this effect. The significance of the delta ferrite content was investigated as follows. Specimens of several of the alloys were brought to phase equilibrium at 925°C, instead of the conventional 1000°C. This resulted in a larger amount of ferrite being present at the soaking temperature. The phase balance at 925°C was determined by VFA of specimens quenched from this temperature. Further specimens of the alloys were then soaked for an hour at 925°C, and cooled to room temperature at 1°C / min. The amount of austenite which was able to transform to ferrite was found by point counting. The results are shown in table 4.6, and indicate that a higher initial ferrite content has a highly significant effect on the transformation kinetics. These results are illustrated in figures 4.12 and 4.13 on pages 63 and 64.

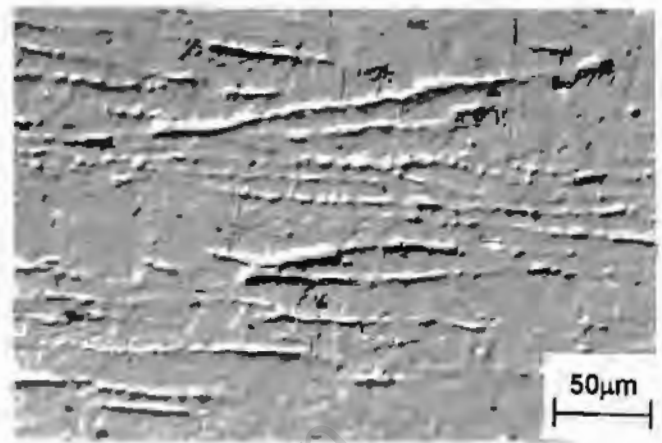
Table 4.6 The effect of initial ferrite content on extent of transformation at 1°C/min.

Alloy no.	Soaking Temp. (°C)	% δ at temp.	% γ at temp.	% α' on cooling	% alpha formed
1	925°C	4,7	95,3	16,7	79
1	1000°C	2,4	97,6	45	53
2	925°C	3,7	96,4	45	51
2	1000°C	0,34	99,66	96,4	3,3
3	925°C	4,8	95,2	57,6	38
3	1000°C	2,3	97,7	84	13
6	925°C	3,6	99,2	48,1	51
6	1000°C	0,8	96,4	87	12
9	925°C	7,1	92,9	78,9	14
9	1000°C	3,1	96,9	93,6	3,3

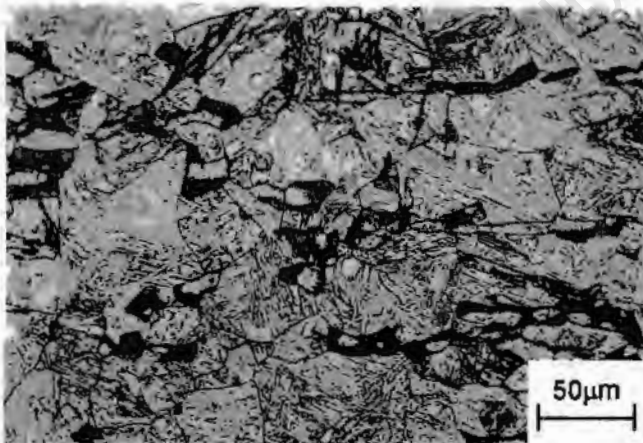
ALLOY 3



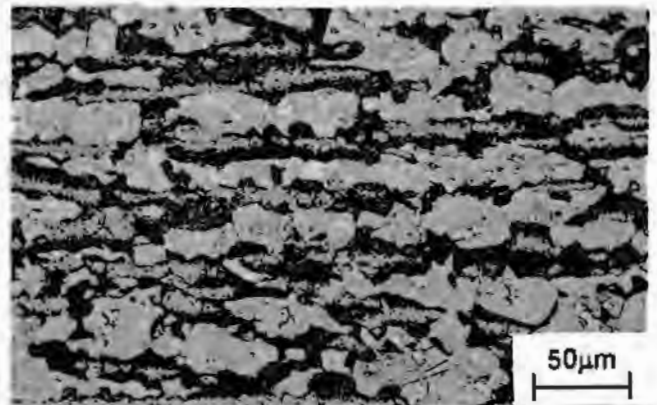
Quenched from 1000°C - 2,3 % ferrite



Quenched from 925°C - 4,8 % ferrite



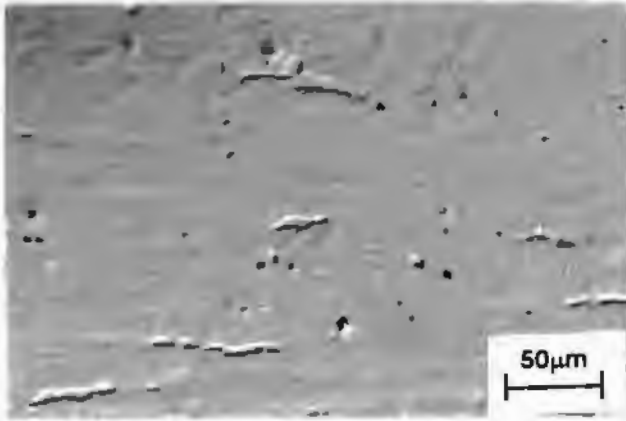
Cooled from 1000°C - 13 % transformation



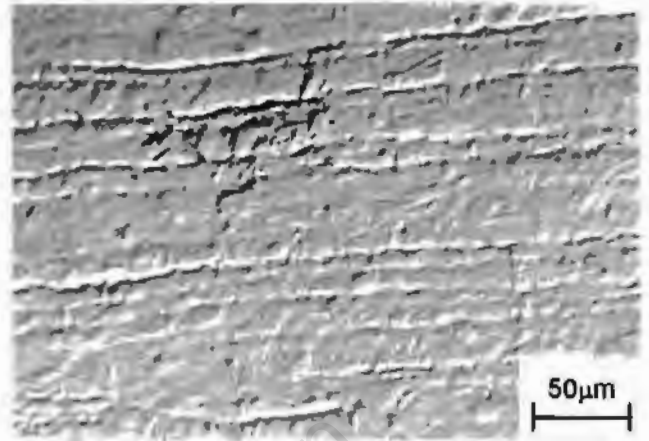
Cooled from 925°C - 38 % transformation

Figure 4.12 The effect of increasing the ferrite content of alloy 3 prior to transformation on the kinetics of the subsequent reaction. In the transformed specimens, the delta ferrite is light grey and the alpha ferrite is dark grey. Martensite is the majority phase. (Quenched specimens etched electrolytically, transformed specimens colour etched.)

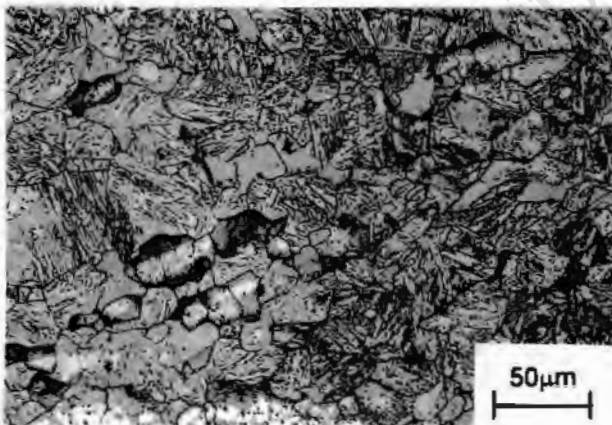
ALLOY 6



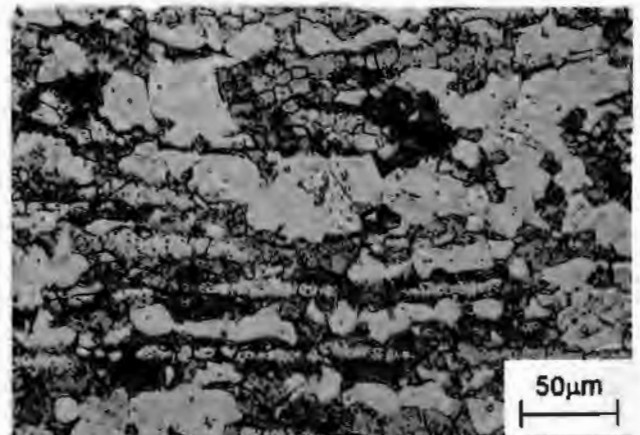
Quenched from 1000°C - 0,8 % ferrite



Quenched from 925°C - 3,6 % ferrite



Cooled from 1000°C - 12 % transformation



Cooled from 925°C - 51 % transformation

Figure 4.13 The effect of increasing the ferrite content of alloy 6 prior to transformation on the kinetics of the subsequent reaction. In the transformed specimens, the delta ferrite is light grey and the alpha ferrite is dark grey. Martensite is the third phase. (Quenched specimens etched electrolytically, transformed specimens colour etched.)

The micrographs of the transformed structures in figures 4.12 and 4.13 reveal two interesting features of the transformation. It is noticeable that the average migration distance of a prior ferrite / austenite boundary is similar in specimens of the same alloy cooled from different soaking temperatures. This is as expected, since the thermodynamics and temperature range of the reaction will not have been altered. In contrast, the transformed structures in figures 4.9 - 4.11 show dramatic changes in the average migration distance as a result of the addition of a single element.

However, the larger initial ferrite content of the specimen soaked at 925°C results in a significant increase in the prior ferrite / austenite interphase area. During transformation, boundary migration can thus be initiated over a far larger surface area, and a correspondingly larger volume of austenite will be able to transform (although the actual migration distance remains the same.)

University of Cape Town

4.4 MECHANICAL PROPERTIES OF 3CR12

4.4.1 Impact Testing Results

Impact toughness tests are a useful way of measuring the microstructural anisotropy of a material. Four of the alloys, with delta ferrite contents at 1000°C ranging from 2,2 to 35 percent, were selected. In order to standardise the microstructures, the as-received plates of about 9mm thickness were brought to equilibrium at 1000°C and then hot rolled to a reduction of 40 %. For each alloy, four sub-standard Charpy specimens, of 3,3 mm thickness, were machined in each of two orientations, L-T and T-L (see figure 2.3).

The results of the tests are shown in table 4.7 below. In all cases, the specimens in the L-T orientation were significantly tougher than those tested in the T-L orientation. From these results, the delta ferrite content of an alloy does not appear to correlate with its toughness.

Table 4.7 Results of impact tests in two perpendicular orientations for 4 of the alloys, with delta ferrite contents at 1000°C ranging from 2,2 to 35 %.

Alloy no.	δ at 1000°C (%)	Orientation	Toughness (J)
4	15	L-T	33 ± 1
4	15	T-L	27 ± 1
7	2,2	L-T	32 ± 2
7	2,2	T-L	21 ± 1
8	6,3	L-T	23 ± 1
8	6,3	T-L	15 ± 1
11	35	L-T	23 ± 2
11	35	T-L	15 ± 1

The anisotropy in toughness for an alloy was determined from the impact values as follows: the difference in the values for the two orientations was divided by half their sum. The results of these calculations are shown in figure 4.14 and indicate that the anisotropy is about 40 % and independent of the delta ferrite content.

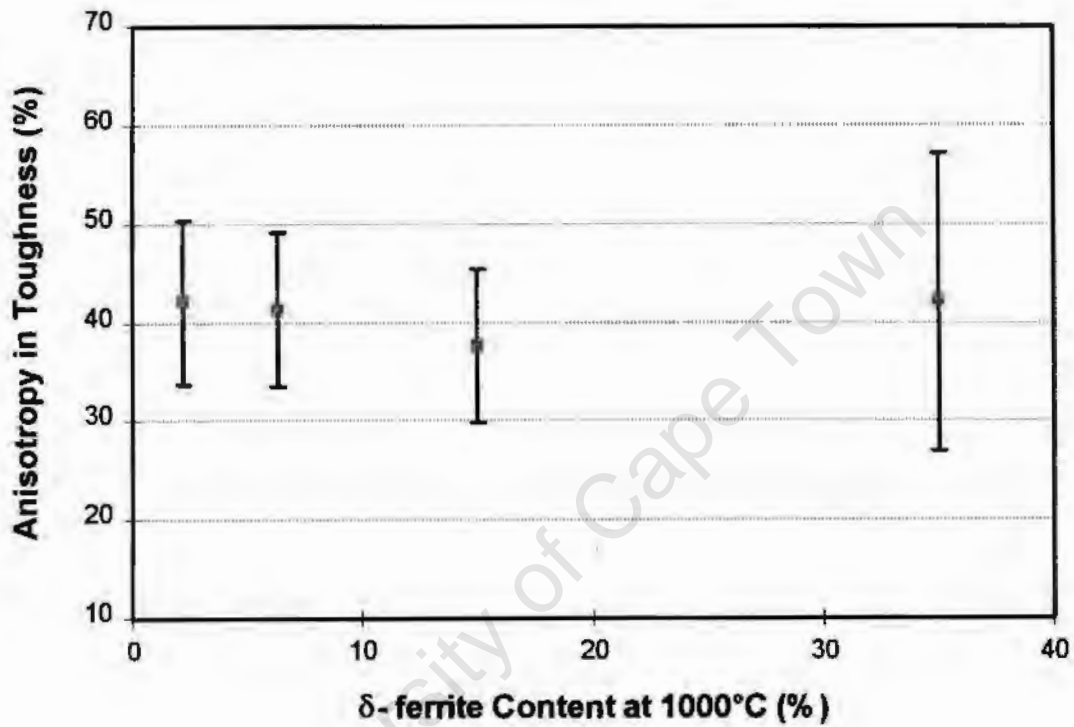


Figure 4.14 Anisotropy in Charpy impact toughness plotted against the delta ferrite content at 1000°C.

4.4.2 Tensile Properties

The percentage elongation, the 0,2% proof stress (PS), and the ultimate tensile strength (UTS) of eight of the alloys were determined. The results are given in table 4.8. The uncertainties shown are the standard deviations of the mean of the three test results.

Comparison of alloy 5 to the base shows that copper has a dramatic effect on the strength of the steel, whilst decreasing its ductility. Cobalt significantly increases the ductility while decreasing the strength, and nickel has the opposite effect. Of the ferrite formers, the addition of Al to alloy 9 increases ductility and decreases strength, whilst silicon has no effect on ductility but leads to a small increase in strength.

Table 4.8 Tensile results for the selected alloys.

Alloy no.	Alloying Elements					% Elong. (in 25mm)	0,2% PS (MPa)	UTS (MPa)
	Co	Cu	Ni	Si	Al			
Base	0,01	0,06	0,41	0,34	0,005	31 ± 1	366 ± 8	484 ± 6
2	1,53	0,07	0,35	0,33	0,001	38 ± 1	317 ± 6	461 ± 2
3	0,02	1,50	0,34	0,41	0,006	25 ± 1	588 ± 6	667 5
4	0,02	1,53	0,33	0,99	0,002	25 ± 1	608 ± 6	694 ± 6
5	1,57	1,53	0,35	0,33	0,001	24 ± 1	613 ± 4	688 ± 3
7	1,58	1,54	0,35	0,33	0,093	28 ± 1	516 ± 1	569 ± 3
9	0,01	0,06	0,94	0,33	0,006	34 ± 1	398 ± 4	534 ± 3
10	0,01	0,06	0,95	0,34	0,151	37 ± 2	307 ± 2	453 ± 1

5. ANALYSIS

5.1 AUSTENITE / FERRITE FORMING ABILITY OF THE ELEMENTS

The electron microprobe (EMP) element partition analysis of section 4.2.3 is an excellent qualitative indication of whether an element is an austenite or ferrite stabiliser. The results show that Co, Cu and Ni, as well as Mn, are austenite stabilisers, whilst Si and Al, as well as Cr, are ferrite formers. The volume fraction analysis (VFA) findings of section 4.2.1, and the dilatometry results of section 4.2.2, support these results and are now analysed further.

5.1.1 Multiple Regression Analysis

The results contained in tables 4.1 and 4.2 have been analysed using multiple regression to obtain a factor for each element representing its relative strength. The factors are shown in table 5.1 below.

Table 5.1 The relative effect of each element on the δ -ferrite content and equilibrium transformation temperatures.

Alloying element	Effect of the addition of 1 % of the element on:		
	δ content (1000°C)	Ae ₁ (°C)	Ae ₃ (°C)
Co	-4,6 %	-10	-16
Cu	-4,3 %	-29	-25
Ni	-2,6 %	-60	-45
Si	+21 %	+54	+42
Al	+80 %	+154	+179

Aluminium is seen to be by far the most potent of the elements, whilst silicon is also a strong ferrite former. Of the austenite stabilisers, cobalt has the greatest effect on the ferrite content, but the weakest effect on the transformation temperatures. Nickel is only a little over half as effective in decreasing the delta ferrite content as Co and Cu, but has the greatest effect in decreasing the transformation temperatures.

The results of Hewitt [4] and Irvine [3] are summarised in table 5.2 for comparison purposes. The results compare relatively well with the results of this thesis, although there are two discrepancies with Hewitt's results. The major discrepancy is Hewitt's finding that aluminium decreases the delta ferrite content by 12 % per unit addition of Al. This contradicts the findings of this work and of Pickering, both of which show Al to dramatically increase the ferrite content at around 1000°C.

A second discrepancy is Hewitt's result for cobalt, which shows the element to be approximately neutral in its effect on delta ferrite content. Both Pickering's values and the results of this investigation show Co to be an austenite former of similar strength to nickel and copper. However, this result is interesting given that cobalt has previously been shown to be both an austenite former and to enhance the decomposition of austenite.

Table 5.2 A summary of the findings of Hewitt and of Pickering with respect to the effects of the elements on δ -ferrite content and the Ac_1 temperature.

Alloying element	Results of Hewitt		Results of Pickering	
	Effect of addition of 1 % of the element on:			
	δ (at 1000°C)	Ac_1 (°C)	δ (at 1050°C)	Ac_1 (°C)
Co	+0,4 %	-21	-7 %	-5
Cu	-24 %	-23	-7 %	-
Ni	-12,6 %	-70	-20%	-30
Si	+32 %	+34	+6 %	+20 to 30
Al	-12 %	+40	+54 %	+30

On a more theoretical basis, these results correspond well with the values of ΔH given in section 2.2 (although cobalt was not included in that list.) Aluminium was found to be a significantly stronger ferrite former than silicon, and copper and nickel were found to be austenite formers of similar strength.

There is no simple theory which is able to explain why each of these elements should have a positive or negative ΔH , as well as its magnitude. A detailed discussion of these results is thus beyond the scope of this thesis, and lies in the electron theory of alloys. However, section 5.1.2 attempts a simple qualitative explanation of the ΔH values of Ni and Cu.

5.1.2 Free Energy and Crystal Structure

The Gibbs free energy of an alloy determines its equilibrium state and is given by:

$$G = H - TS,$$

where H is the enthalpy, T the absolute temperature and S the entropy [22]. The stable state of a system is the one with the lowest free energy. An element is (for example) an austenite former if, when added in equal quantities to both austenite and ferrite, it raises the free energy of the austenite by less than that of the ferrite. When considering the energetics of the addition of an alloying element to ferritic or austenitic iron, it is likely that the crystal structure of the element is of some significance. As discussed below, it appears that elements with a face centred cubic (fcc) structure tend to favour austenite, whilst elements with a body centred cubic (bcc) structure often favour ferrite.

Figure 5.1 shows the crystal structures of some of the elements in the periodic table. Figure 2.9 on page 18 shows, according to the theory of Zener, whether an element stabilises austenite or ferrite. Of the austenite formers, Ni and Cu are fcc, whilst Co and Mn have non-bcc structures. Of the ferrite formers, Cr, Mo, W, Nb, V, and P are all bcc, and Al alone has an fcc structure. Ti, Sn and Si all have other crystal structures. The anomalous behaviour of aluminium may be explained by the fact that it is not a transition element, and thus it will not have a similar electronic structure to austenite or ferrite.

Figure 5.1 A section of rows 3, 4 and 5 of the periodic table, showing the crystal structures of some significant elements.

IIIB	IVB	VB	VIB	VII B	[-VIII-]	IB	IIB	IIIA	IVA		
Sc hex	Ti hex	V bcc	Cr bcc	Mn cube	Fe	Co hex	Ni fcc	Cu fcc	Zn hex	Al fcc	Si diam
Y hex	Zr hex	Nb bcc	Mo bcc	Tc hex	Ru hex	Rh fcc	Pd fcc	Ag fcc	Cd hex	Ga cube	Ge diam
										In tetra	Sn tetra

5.2 KINETICS OF THE $\gamma \rightarrow \alpha$ TRANSFORMATION IN 3CR12

5.2.1 Regression Analysis of Transformation Rate Results

In section 4.3, two methods were used to obtain information regarding the transformation rates of the experimental alloys. The first method used volume fraction analysis and measured how much of the austenite present at 1000°C was able to transform to ferrite when cooled to room temperature at 1°C / min. The second method used dilatometry to measure the cooling rate at which a 4 % volume fraction of alpha ferrite was able to transform.

The results of the first method have been examined using multiple regression in a similar way to the analysis of the results in section 5.1.1. The analysis of the dilatometry results, however, was a little more complicated. The cooling rate for each alloy was divided by the cooling rate found for the base alloy, and then multiplied by 100 (for clarity). The motivation for using the ratio of the cooling rates as the measure of the transformation speed is simply as follows. Consider two alloys, A and B. If the cooling rate found for alloy A is 4°C / min, and for alloy B is 8°C / min, one would say that B transforms twice ($8 \div 4 = 2$) as quickly as alloy A. The results of both the methods, to be analysed using multiple regression, are summarised in table 5.3.

Table 5.3 The results of both the methods used to investigate transformation kinetics.

Alloy no.	Alloying Elements					% alpha formed (at 1°C/min)	Cooling rate (°C / min)	Ratio to base × 100
	Co	Cu	Ni	Si	Al			
Base	0,01	0,06	0,41	0,34	0,005	61,4	27	100
1	0,97	0,07	0,34	0,33	0,001	53	6	22
2	1,53	0,07	0,35	0,33	0,001	3,3	1,5	5,6
3	0,02	1,50	0,34	0,41	0,006	13	3	56
4	0,02	1,53	0,33	0,99	0,002	78	14	15
5	1,57	1,53	0,35	0,33	0,001	0	0,2	0,74
6	1,58	1,51	0,35	0,94	0,001	12	4	11
7	1,58	1,54	0,35	0,33	0,093	97,0	8	30
8	1,58	1,52	0,35	0,92	0,054	93,7	15	52
9	0,01	0,06	0,94	0,33	0,006	3,3	0,7	2,6
10	0,01	0,06	0,95	0,34	0,151	87,1	35	130
11	0,01	0,06	0,94	1,03	0,104	65	40	148

The values obtained from the two methods have been analysed using multiple regression to obtain a factor for each element. The results are shown in the table below.

Table 5.4 The results of the multiple regression analysis, demonstrating the effect of each alloying elements on the transformability of 3CR12.

Alloying element	Effect of the addition of 1 % of the element on:	
	% ferrite formed	Cooling rate ratio
Co	-21	-29
Cu	-14	-35
Ni	-102	-94
Si	+54	+69
Al	+610	+781

This analysis shows that cobalt slows the reaction kinetics by a similar amount to copper, and that nickel has by far the greatest negative effect on transformability. The ferrite formers, Si and Al, both encourage the transformation, with aluminium having the most dramatic effect of all the elements.

5.2.2 Comparison of the Methods Used to Measure Transformation Kinetics of the Alloys

A glance at table 5.3 shows that the results of the two methods differ to a certain extent amongst the alloys. Figure 5.3 plots the position of an alloy in the VFA list against its position in the dilatometry list, with a higher number indicating a faster transformation. (Alloys 8, 10 and 11 have been omitted since they were fully transformed at $1^{\circ}\text{C} / \text{min}$). The two methods are fairly well correlated, with the major area of disagreement being the 3 alloys in the top right hand corner of the graph. It is noticeable that alloy 7, whilst transforming fastest according to volume fraction analysis, is only third fastest when measured by dilatometry. However, it is noticeable that it has the lowest delta ferrite content of the three.

In order to explain this apparent anomaly, a closer look must be taken at exactly what the two methods of ascertaining transformation speed are measuring. Consider first the dilatometric method, which measures the fastest cooling rate at which an inflection point on the dilatometer graph persists. This transformation rate has been found to allow 4 % volume fraction of alpha ferrite to form, which means that the speed at which the first 4 % volume fraction of austenite can decompose is in fact what is being measured. It can be seen that the delta ferrite content should correlate well with these results. The first stage of the growth of alpha ferrite takes place adjacent to delta ferrite / austenite interphase boundaries. A higher delta ferrite content will result in a larger surface area over which movement of the boundary can occur, and thus a smaller migration distance is needed. Alloys 10 and 11, which have by far the highest cooling rates found by dilatometry, confirm this idea: they also have the highest and third highest delta ferrite contents. Alloy 4 is the exception to this rule, having the second highest delta ferrite content but only the fifth fastest cooling rate.

A high delta ferrite content will, of course, also favour the transformation rates measured by VFA. However, it is apparent from figure 5.2 that after the initial period of boundary migration, nucleation of smaller, equiaxed ferrite grains occurs. The migration of the original boundary may be slowed by the build-up of carbon in austenite ahead of the interface. Thus the VFA measurements will be significantly

affected by the ability of the alloy to *sustain* the growth of alpha ferrite, and will be less dependent on the initial delta ferrite content.

The low delta ferrite content may thus be the cause of alloy 7's low rating according to dilatometry, whilst its 0,1 % Al content may be what allows it to sustain the transformation. Linear regression (see figure 5.5) shows that indeed the dilatometry data is more strongly correlated with delta ferrite content ($r^2 = 0,380$) than the VFA results ($r^2 = 0,329$).

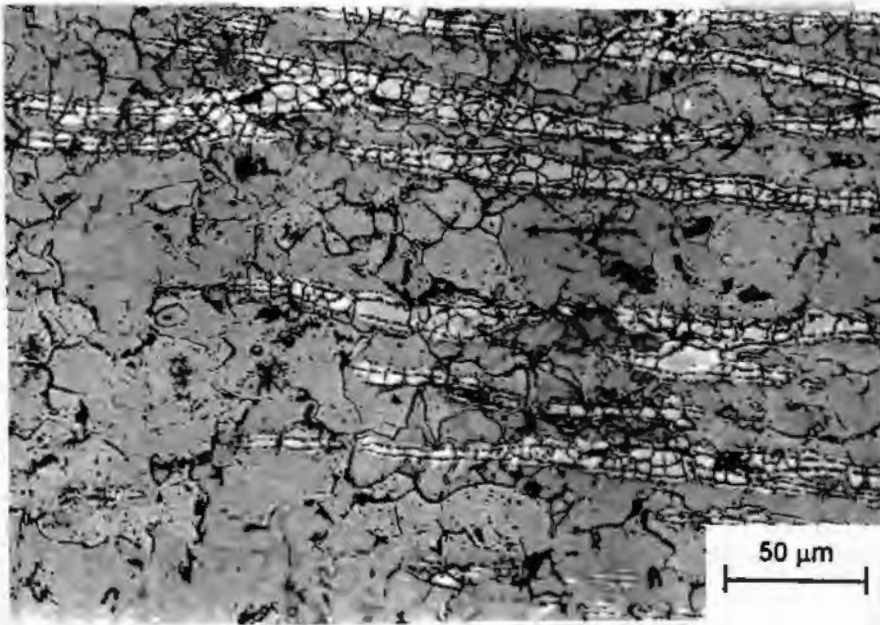


Figure 5.2 Micrograph of alloy 8 cooled at 1°C/min from 1000°C. The initial growth of alpha ferrite (grey) from elongated delta ferrite (light grey) can be seen to have occurred by grain boundary migration. This is followed by the nucleation of equiaxed alpha grains (arrowed) further from the delta ferrite grains.

Comparison Of Methods Used To Measure Transformability

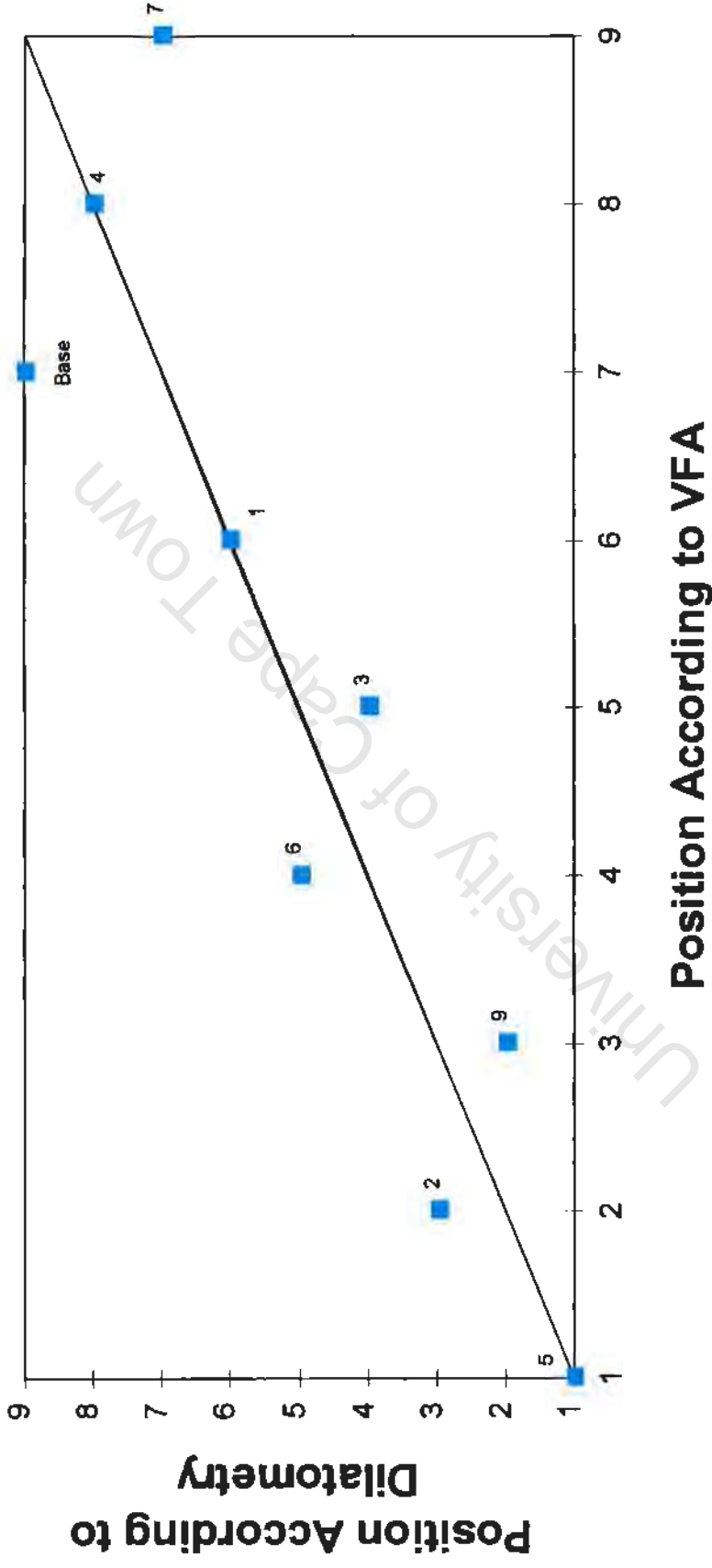


Figure 5.3 The position of the alloy as found by dilatometry is plotted against its position determined by volume fraction analysis (see table 5.3). The points are labelled by the number of the alloy.

5.2.3 Initial Ferrite Content and the Transformation Rate

5.2.3.1 *The effect of increasing the initial ferrite content*

Several authors have noted that increasing the amount of ferrite present prior to the decomposition of austenite encourages the reaction (see section 2.3.1.2.). Figure 5.5 on page 79 shows the transformation rates of sections 4.3.1 and 4.3.2 plotted against ferrite content at 1000°C. The linear fitted curve for the amount transformed indicates an increase in transformation of about 5 % for a 1 % increase in the initial ferrite content. In section 4.3.3, the effect was isolated by transforming the same alloy with different initial ferrite contents. The result was a significant increase in the amount of austenite which was able to transform.

The micrographs in section 4.3.3 clarified the reason for the dramatic acceleration of the transformation. An increase in the volume of ferrite present prior to the onset of cooling leads directly to an increase in the surface area of the ferrite. Since the growth of alpha ferrite occurs (initially) by uniform migration of the delta ferrite / austenite interphase boundaries, an increase in the area of these boundaries will cause an increase in the amount of transformation. The elongated morphology of the delta ferrite grains means that they have a high surface area - to - volume ratio, and this leads to an enhancement of the effect.

The non-linear trendlines fitted to figure 5.5 indicate that the advantage of increasing the initial ferrite content seems to become less significant as the ferrite content gets larger. This effect can be explained, for the volume fraction analysis results, as follows. In section 5.2.2, it was suggested that the most rapid phase of alpha ferrite growth was the initial migration of prior austenite / delta ferrite boundaries. The transformation is then slowed by the build-up of carbon ahead of the interface[25,31], and eventually equiaxed ferrite grains nucleate. In an alloy containing a large amount of delta ferrite at 1000°C, the distance between nearest ferrite grains will be relatively small. This will result in impingement of alpha ferrite grains, as they grow from nearest delta ferrite grains, taking place relatively quickly, often during the rapid grain

boundary migration growth phase (indicated by the thick black arrows in figure 5.4). Transformation in that area of the specimen has thus been completed, but the impingement of alpha ferrite grains during the rapid growth phase means that the full potential of this phase to enhance the transformation has not been realised. In other areas of the alloy, where the distance between nearest delta ferrite grains happens to be relatively large, grain boundary migration will be followed by the slower stage of the transformation, the nucleation of equiaxed alpha ferrite grains (indicated by the thin black arrows in figure 5.4.).

In an alloy with a lower delta ferrite content, the distances between nearest delta ferrite grains will be relatively large. The rapid grain boundary migration growth phase will then be allowed to go to completion in most areas of the specimen (to be followed by the nucleation of equiaxed grains), and the maximum advantage in transformation rate will be realised.

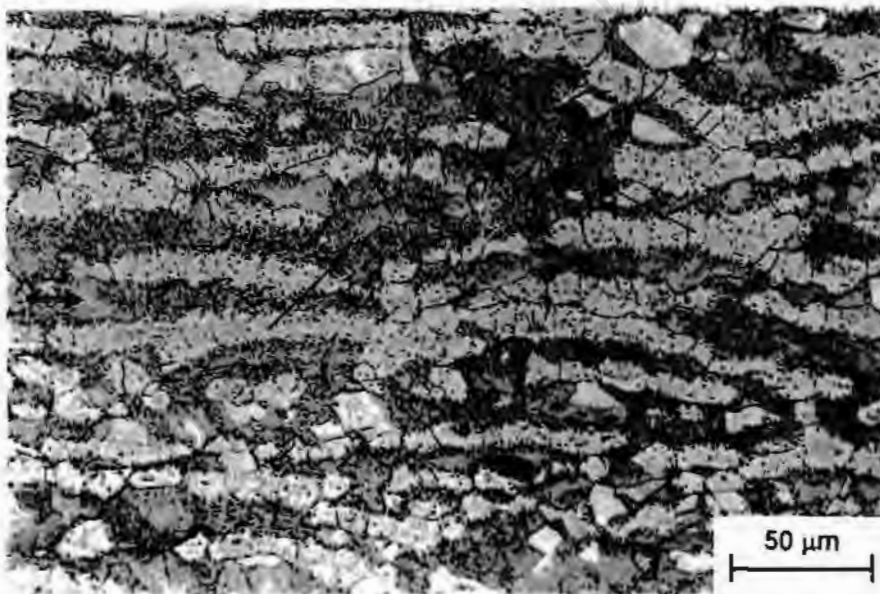


Figure 5.4 Alloy 4 cooled from 1000 °C at 1 °C / min. Impingement of migrating boundaries (indicated by thick black arrows) limits the advantage of a high delta ferrite content. Formation of equiaxed alpha ferrite grains still occurs in some areas (indicated by thin black arrows).

Transformation Rates VS Delta Ferrite Content

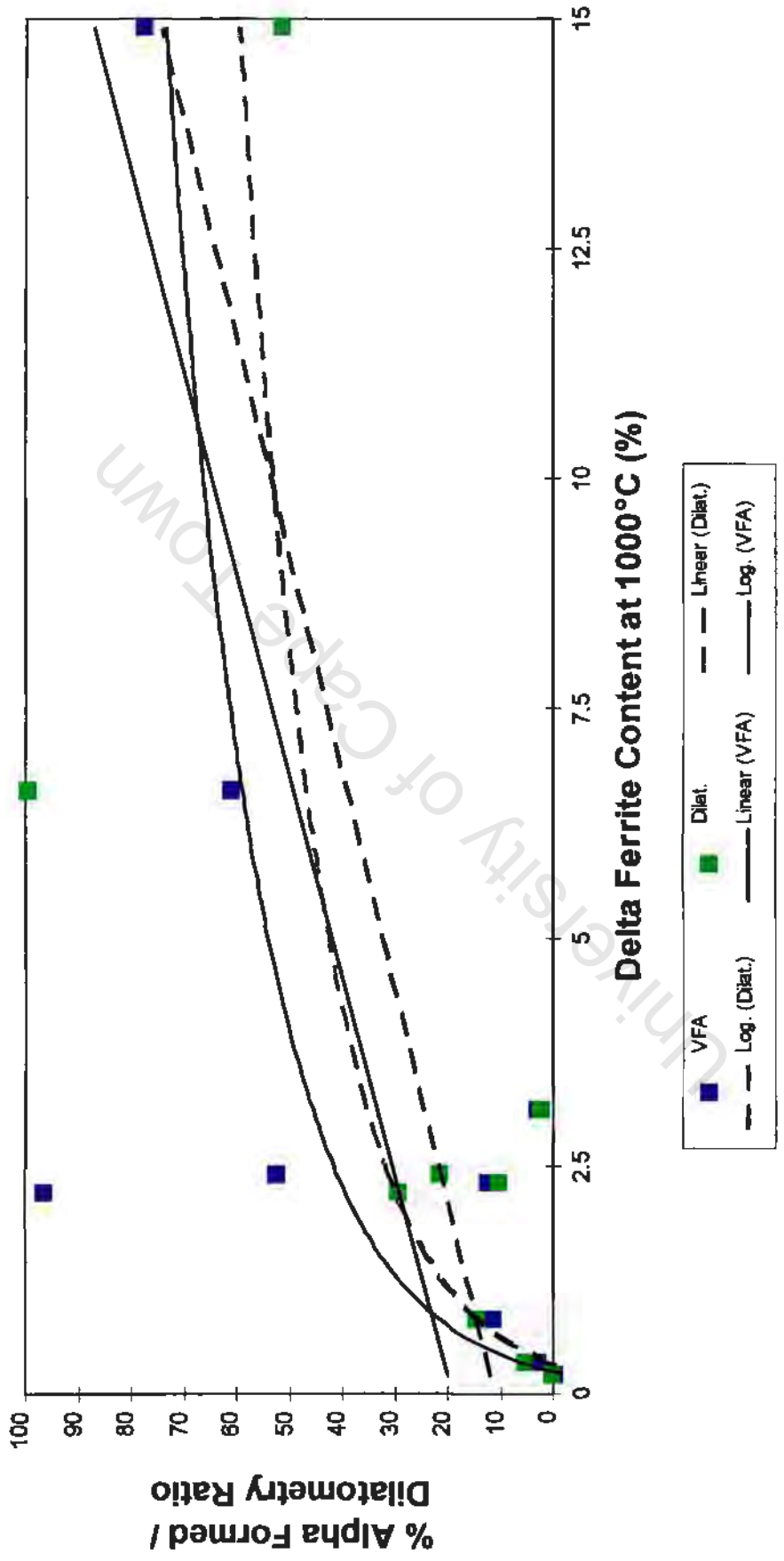


Figure 5.5 The effect of initial ferrite content on the transformation rate. The dashed lines are fitted to the cooling rate values found by dilatometry (dilat.), and the continuous lines are fitted to the amounts transformed as found using volume fraction analysis (VFA).

5.2.3.2 How to adjust for delta ferrite content

The transformation rate analyses of section 5.2.1 give an overall picture of the consequence of adding a particular element. However, they give no indication of why the element has had the observed effect. An attempt will now be made to eliminate the significance of delta ferrite content from the transformation rate results. The results given in table 4.6 (on page 62) provide the necessary data with which to do this. The initial ferrite content of the alloys has been varied by using two different soaking temperatures, but the transformation thermodynamics and temperature range are constant.

The symbol α_T will be used to indicate the amount of alpha ferrite which was able to transform at a cooling rate of 1°C / min from soaking temperature T°C. δ_T will represent the quantity of ferrite present after the alloy has been brought to equilibrium at T°C.

The data in table 4.6, illustrated in figure 5.6 (on page 82) as the green data points, indicate, for the most part, that the larger the increase in ferrite content prior to transformation, the larger the increase in the amount of austenite able to transform (as expected). The results for alloy 9 show that this increase in transformation may level off relatively rapidly with initial ferrite content, also as expected. It would thus seem logical to attempt to correlate the *difference in degree of transformation* ($\alpha_{925} - \alpha_{1000}$) with the *difference in initial ferrite content* ($\delta_{925} - \delta_{1000}$) modified by a factor to account for the actual initial ferrite content (the appropriate data is shown in table 5.5).

Table 5.5 Correlating the increase in transformation with the increase in initial ferrite content.

Alloy no.	δ_{925} (%)	δ_{1000} (%)	α_{925} (%)	α_{1000} (%)	$\frac{\delta_{925} - \delta_{1000}}{\delta_{925}^{0.7}}$	$\frac{\alpha_{925} - \alpha_{1000}}{\alpha_{1000}}$
1	4,7	2,4	79	53	3,4	0,035
2	3,7	0,34	51	3,3	2,5	0,098
5	4,8	2,3	38	13	2,8	0,036
7	3,6	0,8	51	12	2,3	0,088
9	7,1	3,1	14	3,3	4,0	0,020

A trial by error approach was adopted, and the best correlation coefficient was found between the *difference in degree of transformation* and the *difference in initial ferrite content divided by the ferrite content at 925°C raised to the power 2,7*. Linear regression yielded the following equation:

$$(\alpha_{925} - \alpha_{1000}) = 395 \left(\frac{\delta_{925} - \delta_{1000}}{\delta_{925}^{2,7}} \right) + 7,7$$

correlation co-efficient: $r^2 = 0,926$.

The modified values of increase in delta ferrite content are plotted as the blue points in figure 5.6, and the best fit straight line determined above is also shown. The modified values are clearly far more highly correlated with the increase in transformation than is the simple increase in initial ferrite content.

The best fit equation found above can be used to take into account the effect of the initial ferrite content of an alloy on the kinetics of the subsequent transformation, as required. Given the delta ferrite contents of any two of the alloys prior to transformation from 1000°C, the resulting advantage of the one with the larger content can be calculated. The value of δ_{1000} for this alloy is considered to represent δ_{925} in the equation. The difference in the amounts of transformation expected because of the difference in initial ferrite content can then be calculated from the equation, and the transformation rate of the alloy with the lower initial ferrite content compensated accordingly. These calculations have been performed in section 5.2.3.3.

Correlation of Initial Ferrite Content and Transformation Kinetics

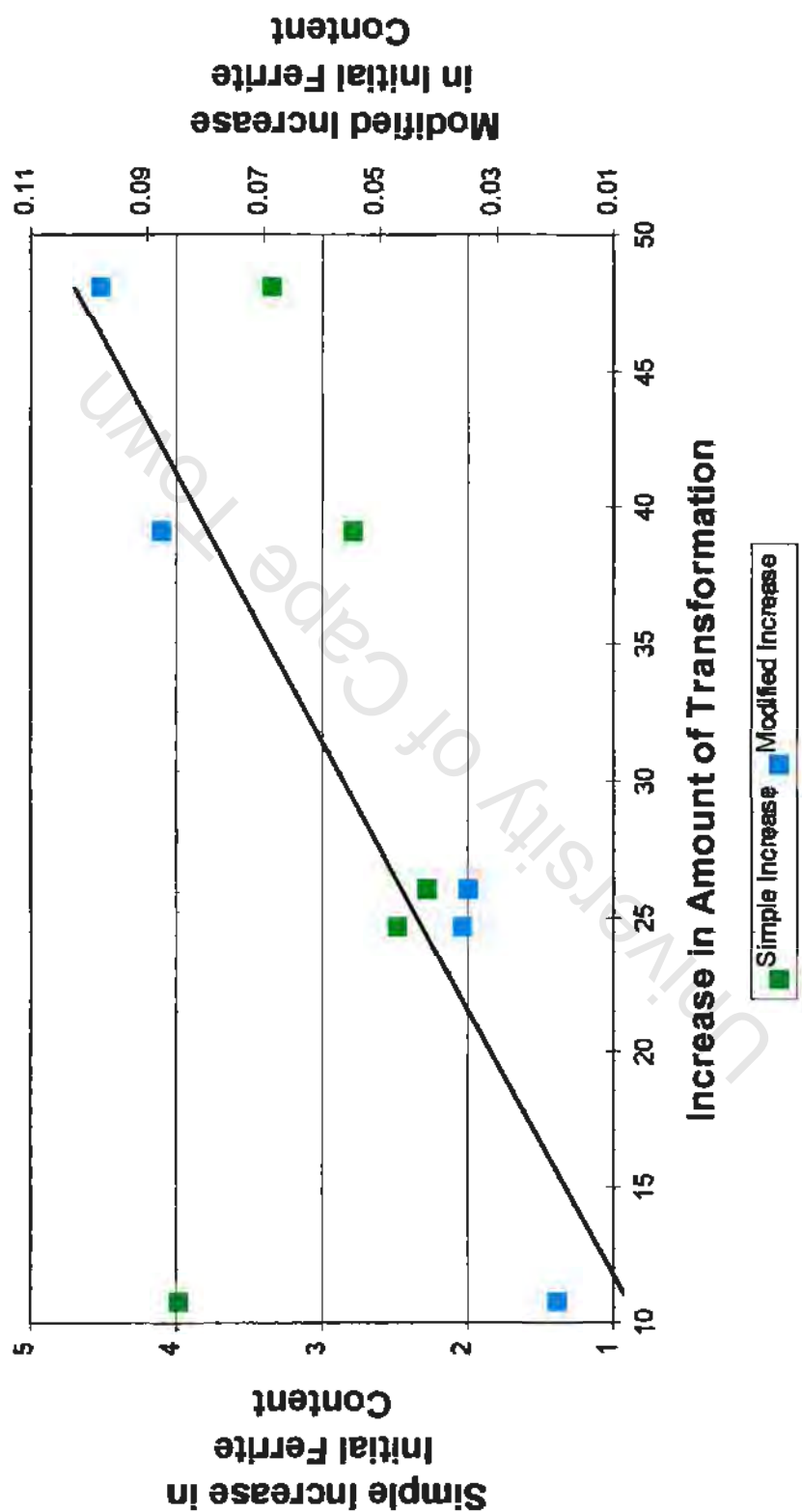


Figure 5.6 The modified increase in initial ferrite content correlates far more significantly with the increase in transformation rate than does the simple increase in initial ferrite content.

5.2.3.3 The transformation rates revisited

The equation was applied by selecting pairs of alloys which differed in a single element. The advantage of the alloy with the greater ferrite content was then calculated, and the α_{1000} value of the alloy with the lower delta ferrite content adjusted accordingly. Only alloys with a delta ferrite content in the range 0,34 - 7,1 % (over which the correction equation was calculated) were considered. The results are shown in table 5.6 below.

Table 5.6 Adjusting the amounts transformed for delta ferrite content.

Element	Alloys compared	δ_{1000} (%)	α_{1000} (%)	Advantage (%)	Adjusted α_{1000} (%)
Cobalt	Base	6,6	61		61
	1: base+0,96 % Co	2,4	53	18	71
Cobalt	Base	6,6	61		61
	2: base+1,52 % Co	0,34	3,3	23	26
Cobalt	1	2,4	53		53
	2: 1+0,56 % Co	0,34	3,3	84	87
Copper	Base	6,6	61		61
	5: base+1,46 % Cu	2,3	13	18	31
Nickel	Base	6,6	61		61
	9: base+0,53 % Ni	3,1	3,3	16	19
Aluminium	7	0,8	12	23	35
	8: 7+0,053 % Al	6,3	94		94

Copper and nickel are confirmed to hinder the decomposition of austenite, and aluminium to enhance it. However, the effect of cobalt is no longer so obvious. The adjusted values for alloy 1 relative to the base, and alloy 2 relative to alloy 1, indicate that Co encourages the transformation, whilst comparison of alloy 2 to the base alloy shows the opposite. It must be noted that the delta ferrite content of alloy 2 (0,34 %) is at the very edge of the allowed range. The most accurate comparison of the three may thus be of alloy 1 to the base.

5.2.4 Transformation Temperatures and Kinetics

5.2.4.1 The effects of alloying elements on transformation temperatures

In section 4.3.1, the transformation temperatures at a cooling rate of $1^{\circ}\text{C} / \text{min}$ were obtained for nine of the alloys. These results were analysed using multiple regression to determine the effects of each element (see table 5.7 below).

Table 5.7 Multiple regression analysis of the transformation temperatures.

Alloying element	Effect of addition of 1 % of element on:	
	Ar_1 ($^{\circ}\text{C}$)	Ar_3 ($^{\circ}\text{C}$)
Co	-11	-15
Cu	-38	-40
Ni	-203	-69
Si	+80	+55
Al	+646	+285

Due to the limited number of observations, these results are not considered to be highly accurate. This applies especially to nickel, for which only 3 of the additions differed significantly from the base alloy.

The above multiple regression results were used to obtain the Ar_1 and Ar_3 temperatures of the alloys which did not transform substantially enough at $1^{\circ}\text{C} / \text{min}$ for their transformation points to be determined from a dilatometer curve. These temperatures are needed for further analysis of the $\gamma \rightarrow \alpha$ reaction. For each of these alloys, the alloy in table 4.4 with the most similar composition was selected. The regression factors determined above were then used to find the transformation points.

Table 5.8 The transformation temperatures of three of the alloys, determined by combining the multiple regression factors of table 5.7 with results obtained for another alloy (which is shown in brackets).

Alloy no.	Alloying Elements					Ar_1 ($^{\circ}\text{C}$)	Ar_3 ($^{\circ}\text{C}$)
	Co	Cu	Ni	Si	Al		
2 (1)	1,53	0,07	0,35	0,33	0,001	578	764
3 (4)	1,57	1,53	0,35	0,33	0,001	536	707
9 (base)	0,01	0,06	0,94	0,33	0,006	539	757

5.2.4.2 Transformation Ranges and the Diffusion of Carbon

The arithmetic mean of the Ar_1 and Ar_3 temperatures, Ar_m , can be used as an approximate "average temperature" for the transformation range of an alloy. The ratio of the arithmetic mean, expressed in units of Kelvin, of each alloy with respect to the base alloy value was calculated, and multiplied by 100 for convenience. The results are shown in the second from right hand column of table 5.9 on page 86.

The variation in these values is relatively small, with a typical difference between two alloys being two or three percent. The largest difference, of 10 %, is between alloy 2 and alloy 11.

However, the true effect of temperature may be significantly more important than this. It was shown in section 4.1.4 that partition of substitutional alloying elements does not take place during the transformation of 3CR12 type alloys at $1^\circ\text{C} / \text{min}$. The diffusion rates of the interstitials, carbon and nitrogen, is thus the significant factor in so much as the rate of the transformation is diffusion controlled. The diffusion coefficient, D , for interstitial diffusion is given [38] by the Arrhenius-type equation:

$$D = D_0 \exp\left(\frac{-Q}{RT}\right)$$

where D_0 is a material constant, Q is the activation enthalpy, T is the absolute temperature and R is the universal gas constant. It is significant that this relationship has an exponential dependence on temperature, as opposed to the linear relationship assumed when comparing the arithmetic means of the transformation temperatures.

Consider any two of the alloys used in this work, alloy A and alloy B, transformed at $1^\circ\text{C} / \text{min}$. The arithmetic means of their Ar_1 and Ar_3 temperatures are again considered as approximate "average temperatures" at which they transform, and are designated T_A and T_B . The ratio of the interstitial diffusion coefficients for the two alloys can then be shown to be given by:

$$\frac{D_A}{D_B} = \exp\left(\frac{Q(T_A - T_B)}{RT_A T_B}\right)$$

where $T_A > T_B$. The activation enthalpy for C in austenitic iron has been determined as 135 kJ / mol respectively [25].

The ratio of the diffusion constants of C in each alloy with respect to the base alloy have been calculated and are shown in the right hand column of table 5.9, and again have been multiplied by 100. These results show a significant amount of variation amongst the alloys of carbon diffusion rates during transformation.

Table 5.9 The variation in A_{r_m} and carbon diffusion coefficient, resulting from the effects of the elements on the transformation range.

Alloy no.	Alloying elements					A_{r_m} (K)	A_{r_m} ratio	$D_{C_{alloy}}/D_{C_{base}}$
	Co	Cu	Ni	Si	Al			
Base	0,01	0,06	0,41	0,34	0,005	992	100	100
1	0,97	0,07	0,34	0,33	0,001	953	96	51
2	1,53	0,07	0,35	0,33	0,001	944	95	43
3	0,02	1,50	0,34	0,41	0,006	895	90	17
4	0,02	1,53	0,33	0,99	0,002	937	94	38
5	1,57	1,53	0,35	0,33	0,001	950	96	48
6	1,58	1,51	0,35	0,94	0,001	944	95	43
7	1,58	1,54	0,35	0,33	0,093	936	94	37
8	1,58	1,52	0,35	0,92	0,054	995	100	104
9	0,01	0,06	0,94	0,33	0,006	921	93	28
10	0,01	0,06	0,95	0,34	0,151	959	97	57
11	0,01	0,06	0,94	1,03	0,104	1004	101	121

To isolate the effects of the elements, linear regression was performed on both the A_{r_m} and the diffusion coefficient ratios (see table 5.10). The effects of the elements on the diffusion rate of carbon appears to be highly significant. The true effect of the transformation range on the kinetics is probably greater than indicated by the "average" transformation temperatures, but less than that suggested by the carbon diffusion coefficients.

Table 5.10 The effects of the elements on the A_{r_m} ratio and the carbon diffusion coefficient ratio.

Alloying element	Effect of addition of 1 % of the element on:	
	A_{r_m} Ratio	$D_{C_{alloy}}/D_{C_{base}}$
Co	-1,6	-11
Cu	-3,4	-31
Ni	-11	-84
Si	6,5	67
Al	41	345

5.2.5 Summary

In section 2.3.1, the following six ways in which alloying elements might effect transformation kinetics were suggested:

- i) Thermodynamics
- ii) Delta ferrite content prior to transformation
- iii) Interphase boundary precipitation (IBP)
- iv) Solute drag-like effect (SDLE)
- v) Elevation of reaction temperature
- vi) Element partition

An investigation of the SDLE was beyond the scope of this thesis, whilst electron microprobe analysis showed that element partition did not occur during transformation. Although there was some evidence for IBP, there is anyway little consensus on what consequences this would have for transformation kinetics. The effects of the elements on kinetics will thus be discussed in terms of the other 3 factors.

The negative effect of Cu and Ni seems to be a combination of lowering the transformation range, thermodynamic favouring of austenite and decreasing the delta ferrite content.

In section 5.2.3.3 it was suggested that after allowing for delta ferrite content, Co might enhance the transformation kinetics. Since cobalt has been shown to lower the temperature range of transformation, which should slow the kinetics, there is evidence that the element may in fact thermodynamically favour the transformation to ferrite.

Si was found to encourage the decomposition of ferrite. This will certainly in part be due to an increase in delta ferrite content and the transformation range, but is probably also due to thermodynamic effects.

Al was shown to strongly increase the kinetics of the decomposition to austenite even after factoring in its expansion of the delta ferrite content. Although the corresponding increase in the temperature range will help, aluminium appears to strongly favour ferrite in thermodynamic terms.

5.3 DISCUSSION OF MECHANICAL PROPERTY RESULTS

5.3.1 Toughness and Specimen Orientation

There were two interesting aspects of the impact testing results of section 4.4.1. The first was that the L-T specimens are in all cases tougher than the T-L specimens. The second was that this anisotropy is not affected by the delta ferrite content. These observations can be discussed in terms of the crack-divider theory of Embury reviewed in section 2.1.3.

Bramfitt and Marder [18] found that T-L Charpy specimens exhibited more laminations than L-T specimens, indicating that splitting occurs more easily in T-L specimens. Matthews et al [17] performed measurements of grain size in 3CR12, the results of which are shown in table 5.11. The pancake shaped grains of rolled 3CR12 are thus more elongated in the longitudinal direction than the transverse direction. This result is the most likely explanation for why splitting should occur more easily in one orientation than another.

Following the theory of Embury, if splitting occurs more easily in T-L specimens, then this orientation should have lower shelf energies, which is what the results in section 4.4.1 state.

Table 5.11 Grain size measurements in 3CR12.

Direction Measured	Length (micrometers)	Standard Deviation
Rolling	29,46	1,02
Transverse	22,93	1,14
Thickness	14,65	0,82

If the delta ferrite content in 3CR12 is altered, the lengths of grains in the rolling, transverse and thickness directions will change. However, it can be expected that the changes will be roughly in proportion and that the delta ferrite grains will remain more elongated in the rolling direction than the transverse direction. Thus splitting will occur more easily in the T-L specimens, no matter what the delta ferrite content. Only the complete absence of delta ferrite can be expected to remove the anisotropy in toughness between the T-L and L-T orientations.

5.3.2 Regression Analysis of Tensile Results

The tensile results of table 4.8, for specimens in the hot-rolled, annealed condition, were analysed using multiple linear regression. Since only eight observations were available, the results (shown in table 5.12) may not be as accurate as desired. This applies especially to silicon, for which only one of the alloys had a content significantly different to the base.

Table 5.12 Multiple regression analysis of the tensile results of table 4.8.

Alloying element	Effect of addition of 1 % of the element on:		
	Elongation (%)	0,2 % PS (MPa)	UTS (MPa)
Co	+2	-13	-8
Cu	-7	+181	+137
Ni	+1	+108	+135
Si	+4	-3	+34
Al	24	-738	-779

The regression output appears to be relatively accurate, with the exceptions that Si seems to increase rather than decrease the proof stress and have no effect on ductility, and that the action of cobalt in increasing the ductility and decreasing the strength have been underestimated.

The figures for nickel are interesting in that it leads to a significant increase in strength, but may also increase the ductility. Copper causes a similar increase in strength, and has the more conventional effect of a corresponding decrease in ductility. Aluminium and cobalt have the reverse effect of increasing ductility and decreasing strength, with aluminium having by far the greater effect.

6. CONCLUSIONS

6.1 EFFECTS OF THE ELEMENTS

1. Nickel has been shown to act as an austenite stabiliser and to slow the transformation rate. It has a significantly stronger inhibitive effect on the decomposition of austenite than Cu or Co. It significantly increases the strength of the steel without a corresponding decrease in ductility.
2. Copper is an austenite stabilising element of similar strength to Ni, but does not slow the transformation kinetics to such an extent. Cu was found to precipitate out of solution during cooling from 1000°C, both within delta ferrite stringers and newly formed alpha ferrite. It notably increases the strength of the steel but causes a decrease in ductility.
3. Cobalt was found to act as a conventional austenite forming element at 1000°C. However, after allowing for delta ferrite content during transformation, and reaction temperature range, there is evidence to suggest that cobalt may thermodynamically enhance the transformation kinetics. A possible explanation for these seemingly contradictory results is that Co, having a different crystal structure to both austenite and ferrite, may thermodynamically favour the fcc phase at higher temperatures, and the bcc phase at lower temperatures. Cobalt increases the ductility and decreases the strength of the alloy.
4. Silicon acts as a ferrite stabilising element, and enhances the kinetics of the decomposition of austenite. This is due to a combination of an increase in the delta ferrite content, an increase in the transformation temperature range, and thermodynamic effects. Silicon may slightly increase the strength of the alloy without a corresponding decrease in ductility.

5. Aluminium acts as a very strong ferrite stabilising element, and dramatically increases the transformability of the steel. This is due to a combination of raising the delta ferrite content and the transformation temperature range, and strongly favouring ferrite thermodynamically. Aluminium forms precipitates in a similar way to Cu and Si. Al greatly decreases the strength and increases the ductility of the alloy.

6.2 GENERAL CONCLUSIONS

1. An increase in delta ferrite content prior to transformation leads to a highly significant increase in transformation kinetics. This is due to the increase in delta ferrite / austenite interfacial area, from which boundary migration may proceed during the growth of alpha ferrite. Attempting to minimise the delta ferrite content will thus significantly slow the transformation kinetics.

2. The elemental additions result in significant variation in the transformation temperature ranges of the alloys, which will affect diffusion rates and consequently the reaction rates.

3. The delta ferrite content has no effect on the impact toughness anisotropy between the L-T and T-L orientations of about 40 %. However, the toughness of 3CR12 in these two orientations is considered more than adequate.

4. The primary objectives of this thesis were defined in the introduction as follows:

- To minimise the delta ferrite content of the steel during hot rolling.
- To improve the transformability of 3CR12 so that a fully ferritic structure can be obtained after air cooling.

However, it was found that all five of the elements investigated in this thesis either increase the delta ferrite content or slow down the transformation rate. (Although cobalt may thermodynamically favour the formation of alpha ferrite, its overall effect is to slow the transformation kinetics.) For this reason, it is unlikely that both the main objectives of this thesis can be achieved. A compromise will have to be sought between eliminating anisotropy and increasing transformability.

REFERENCES

1. BALL A and HOFFMAN J P, *Met. Technol.*, 1981, **8**, (9), 329-338.
2. PICKERING F B, *Int. Metals. Rev.*, 1976, Review **211**, 227-268.
3. IRVINE J K, CROWE D J and PICKERING F B, *JISI*, 1960, **195**, 386.
4. HEWITT J, Proc. 1st Int. Chromium Steels and Alloys Congress, Cape Town (1992), SAIMM, Johannesburg, 1992, 71-88.
5. PISTORIUS P G H, PhD. Thesis, Univ. of Pretoria, 1992.
6. PISTORIUS P G H, DE KLERK H J and VAN ROOYEN G T, Proc. 1st Int. Chromium Steels and Alloys Congress, Cape Town (1992), SAIMM, Johannesburg, 1992, 65-70.
7. BALL A, CHAUHAN Y and SCHAFFER G B, *Mat. Sci. and Technol.*, 1987, **3**, 189-196.
8. BRINK A B, MSc. Thesis, Univ. of Cape Town, 1983.
9. HOFFMAN, J P, 1984 ASM Int. Con. on New Developments in Stainless Steel Technology, Detroit, Michigan, 1984, paper 8410-014.
10. ZAAYMAN J J J and VAN ROOYEN, G T, Proc. 1st Int. Chromium Steels and Alloys Congress, Cape Town (1992), SAIMM, Johannesburg, 1992, 137-142.
11. PROZZI J M and VAN ROOYEN G T, Proc. 1st Int. Chromium Steels and Alloys Congress, Cape Town (1992), SAIMM, Johannesburg, 1992, 123-128.
12. BELYAKOV A, KAIBYSHEV, R and ZARIPOVA R, *Materials Science Forum*, 1993, **113-115**, 385-390.
13. ZARIPOVA R G, KAIBYSHEV O A and SALISHCHEV G A, *The Physics of Metals and Metallography*, 1992, **73**(4), 415-421.
14. GROBLER C and VAN ROOYEN G T, *Can. Metall. Q.*, 1988, **27**(1), 49-58.
15. EMBURY J D, PETCH N J, WRAITH A E and WRIGHT E S, *Trans. Metall. Soc. A.I.M.E.*, 1967, **239**, 114.
16. CORTIE M B, FLETCHER C J and VELDSMAN W, Proc. 1st Int. Chromium Steels and Alloys Congress, Cape Town (1992), SAIMM, Johannesburg, 121-129.

17. MATTHEWS L M, NANA S and CORTIE M B, Proc. Fracture '89, 3rd Nat. Con. on Fracture, Univ. of the Witwatersrand, Johannesburg, June 1989.
18. BRAMFITT, B L and MARDER A R, *Metallurgical Transactions A*, 1977, **8A**, 1263-1273.
19. SCHAFFER G B, MSc. Thesis, Univ. of Cape Town, 1983.
20. KNUTSEN R D, *Mat. Sci. and Technol.*, 1992, **8**, 621-627.
21. SARATH KUMAR MENON E and AARONSON H I, *Acta Metall.*, 1987, **35**, 3, 549-563.
22. CAHN R W and HAASEN P, *Physical Metallurgy*, 3rd edn., 1983, North-Holland Physics Publishing, Amsterdam.
23. ZENER C, *Trans. Amer. Inst. Min. Met. Eng.*, 1946, **167**, 513-534.
24. TANAKA T, ARONSON H I and ENOMOTO M, *Metall. Mater. Trans. A*, 1995, **26A**, 561-580.
25. HONEYCOMBE R W K, *Steels Microstructure and Properties*, 1981, Edward Arnold, London.
26. SCHAEFFLER A L, *Welding Journal*, Oct. 1947, **26**, 601s-620s.
27. MARSHALL P, *Austenitic Stainless Steels Microstructure and Mechanical Properties*, 1984, Elsevier Applied Science Publishers, London.
28. PORTER D A and EASTERLING K A, *Phase Transformation in Metals and Alloys*, 2nd edn., 1992, Chapman and Hall, London.
29. PISTORIUS P G H and VAN ROOYEN G T, Proc. of Innovation Stainless Steel, Florence, Italy, 1993.
30. KOEPKE V W, SKUIN K and HERFERT S, *Neue Hutte*, 1970, **15(3)**, 165-170.
31. DAVENPORT A T and BECKER P C, *Metall. Trans.*, 1971, **2**, 2962.
32. GRAY J M and YEO R B G, *Trans. ASM*, 1968, **61**, 255.
33. HOWELL P R, RICKS R A, BEE J V and HONEYCOMBE R W K, *Phil. Mag. A*, 1980, **41**, 165.
34. BHADESHIA H K D H, *Prog. Mater. Sci.*, 1985, **29**, 321-386.
35. BRADLEY J R and AARONSON H I, *Metall. Trans. A*, 1981, **12A**, 1729-1741.

36. SHIFLET G J, AARONSON H I and BRADLEY J R, *Metall. Trans. A*, 1981, **12A**, 1743-1750.
37. AARONSON H I and DOMIAN H A, *Trans. Metall. Soc. A.I.M.E.*, 1966, **236**, 781-796.
38. PHILIBERT J, Atomic Movements Diffusion and Mass Transport in Solids, 1991, Les Editions de Physique, France.
39. MOSTERT J R and VAN ROOYEN G T, *Mat. Sci. and Technol.*, 1991, **7**, 803-811.
40. AARONSON H I, DOMIAN H A and POUND G M, *Trans. Metall. Soc. A.I.M.E.*, 1966, **236**, 768-781.
41. KINSMAN K R and AARONSON H I, *Metall. Trans.*, 1973, **4**, 959.
42. CURE J, *Traitement Thermique*, 1968, **36-68**, 71-80.
43. BERAHA E and SHPIGLER, *Color Metallography*, 1977, ASM, Metals Park, Ohio.
44. HILLIARD J E, Proc. Fourth Int. Con. for Stereology, NBS, Gaithersburg, Md., 1975.
45. EXNER H E, Proc. Fourth Int. Con. for Stereology, NBS, Gaithersburg, Md., 1975.
46. VOORT V D, *Metallography Principles and Practice*, 1984, McGraw-Hill, New York.
47. UNDERWOOD E E, *Quantitative Stereology*, 1970, Addison-Wesley.
48. KIRKALDY J S and BAGANIS E A, *Metall. Trans. A*, 1978, **9A**, 495-501.